COLD FUSION BY SPARKING IN HYDROGEN ISOTOPES

JACQUES DUFOUR *Shell Research S. A., Route de Caen F-76530 Grand-Couronne, France*

COLD FUSION

TECHNICAL NOTE

KEYWORDS: *sparks, metallic hydrides/deuterides, radiation emission*

Received November 18, 1992
Accepted for Publication February 22, 1993

Excess energy production, well above the background and in amounts of the same order of magnitude as the input energy, has been measured that has been caused by sparking in hydrogen isotopes between electrodes made of metallic hydride-forming metals (palladium and stainless steel). This excess energy production is stable over long periods (several weeks) and is observed with both hydrogen and deuterium. Only extremely low levels of neutrons and tritium have been detected, many orders of magnitude below what would be expected from the excess energy production measured. On the contrary, copious emission of low-energy radiation (likely to be beta rays) has been observed.

A class of hypothetical nuclear reactions, based on the action of the weak electronuclear force, is proposed that accounts for all the experimental facts observed.

I. INTRODUCTION

In 1989, observations of excess energy generation during the course of heavy water electrolysis with a palladium cathode, were reported[1,2] and attributed to possible nuclear fusion reactions of the deuterium stored in the palladium, through the action of the electrolysis. These reactions were claimed to be caused by the very high pressure to which the deuterium would be subjected in palladium highly loaded with deuterium, which would favor tunneling through the Coulomb barrier. Evidence was presented of neutron emission and tritium production that were several orders of magnitude lower than what would be expected from the observed energy production. As early as 1926 and 1927, ways to cause nuclear fusion reaction of deuterium to yield ^{4}He had been discussed.[3,4]

Following the 1989 announcement, many experiments were run in an attempt to reproduce this observation and to identify nuclear by-products, a number of which gave negative results.[5-8] Researchers also tried to trigger these fusion reactions by creating non-steady-state situations in metals (titanium and palladium) loaded with deuterium: temperature and pressure variations were tried by various teams.[9-11] Researchers also tried using a deuterium plasma; one of the electrodes used to generate the plasma was made of palladium.[12-14]

In parallel, various possible mechanisms were proposed to try to explain how fusion reactions could occur at room temperature despite the high Coulomb barrier to be overcome.[15-18] Some doubts were expressed regarding the ability of pressure[19] or electron concentration[20] to overcome the Coulomb barrier. A very good comprehensive review of the status of cold fusion at the end of 1991 is given in Ref. 21.

After 2 yr, interest in the subject decreased, mainly for three reasons:

1. The energy generation is not reproducible and occurs under unpredictable circumstances.

2. The observed signs of nuclear reactions are not in line with what would be expected from known fusion reactions.

3. No fully acceptable reaction mechanism has so far been proposed that can justify any novel fusion reactions that could account for all the experimental observation.

This technical note presents an original approach that was started in May 1989 and on which a patent was filed in July 1989 (Ref. 22). We report significant and fully reproducible excess energy production and present a possible cold fusion reaction scheme of hydrogen isotopes that is justified by the fundamental properties of quantum mechanics and accounts for experimental facts that have been observed in our experiments.

II. CONCEPT USED AND MAIN RESULTS

A concept different from electrolysis is used: the action of a high transient electrical field on hydrogen isotopes concentrated in the surface layer (few micrometres) of a metal in contact with a gaseous mixture containing hydrogen isotopes.

The transient electrical field is created by sparking through the gas between two dissymmetrical electrodes, in which the surface layer of hydrogen isotopes is built. The accumulation of these species in a surface layer of the metal used as the electrode can be explained by known properties of sparks and of hydrogen isotopes in metals.

Precise and repeated energy balances show that excess energy is generated in the system, in a fully reproducible way. The amount measured on a steady-state basis (several days)

excludes chemical or physical explanations. This excess energy production is observed with both hydrogen and deuterium and with various metals, even those forming unstable hydrides (iron, nickel), indicating a surface reaction.

On the basis of electrical energy input to the reactor, energy breakeven has been obtained (taking into account an efficiency of 50% for electricity generation). Excess energy production of up to 2.5 W has been measured.

The known properties of spark discharges clearly indicate how the energy efficiency of the process could be increased.

Indications of the emission of β^- particles have been observed. In contrast, there has been no evidence (or only exceedingly small signs) of the classical fusion reactions of hydrogen isotopes (practically no tritium and no neutrons were detected).

Taking into account the fundamental properties of quantum mechanics, it can be shown that a whole class of nuclear fusion reactions at room temperature, involving hydrogen isotopes, are allowed through an indirect transition (virtual neutron state). These reactions are favored by the high electron and proton concentrations existing in the metal and the high transient electrical field created by the sparks. They implicate the weak electronuclear force and yield products completely different from those of hot fusion. Experimental evidence is presented that supports the occurrence of these reactions and that explains all the features observed in our experiments.

It remains to be demonstrated whether the probability of these reactions can be brought to a sufficiently high level to justify their utilization in energy production.

III. EXPERIMENTAL

The reaction is carried out in a reactor as presented in Fig. 1. The reactor can be connected through a manifold to a gas cylinder containing deuterium, nitrogen, hydrogen, or argon (see gas analysis in Table I) or a vacuum pump (Alcatel 1004 A). This enables controlled flushing and filling of the reactor (see Fig. 2). Sparking takes place between two dissymmetrical electrodes: one 1-cm-diam × 2.4-cm-high × 0.5-mm-thick cylindrical electrode connected to and supported by a 1-cm-diam copper tube (which is one of the armatures of a

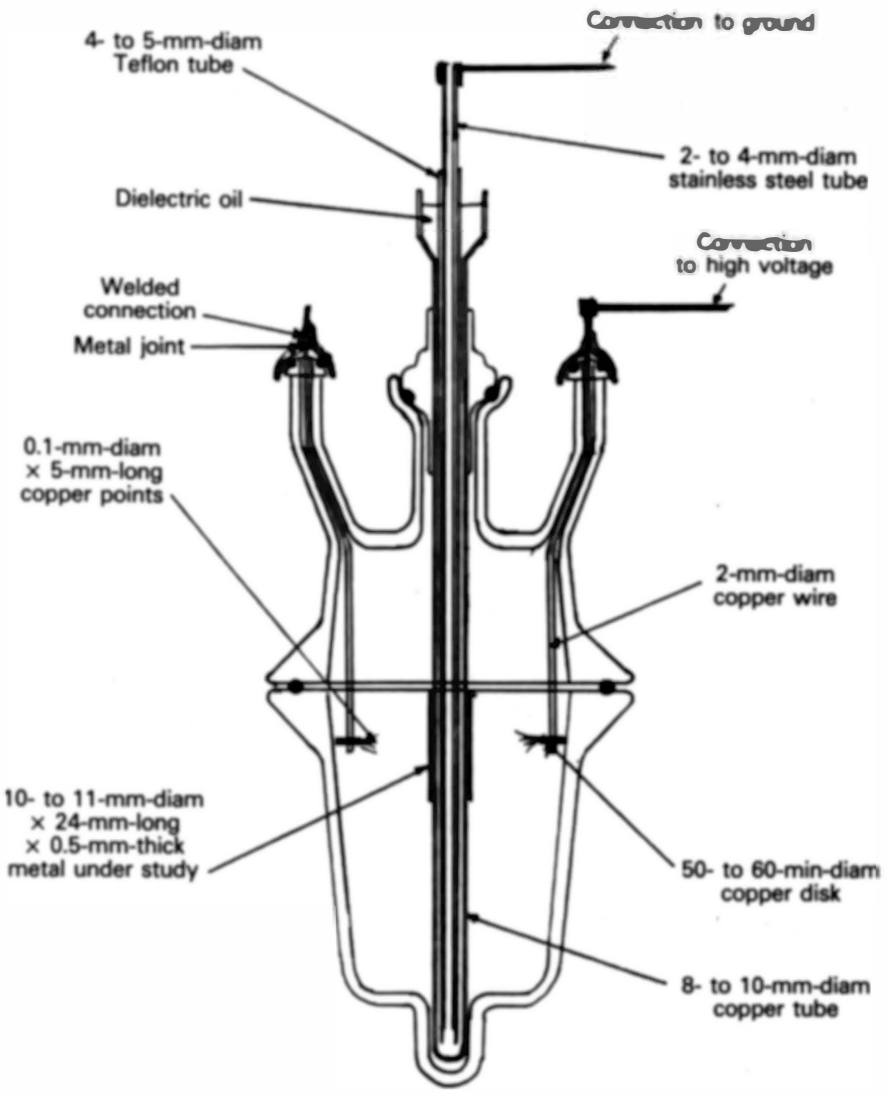

Fig. 1. Reactor.

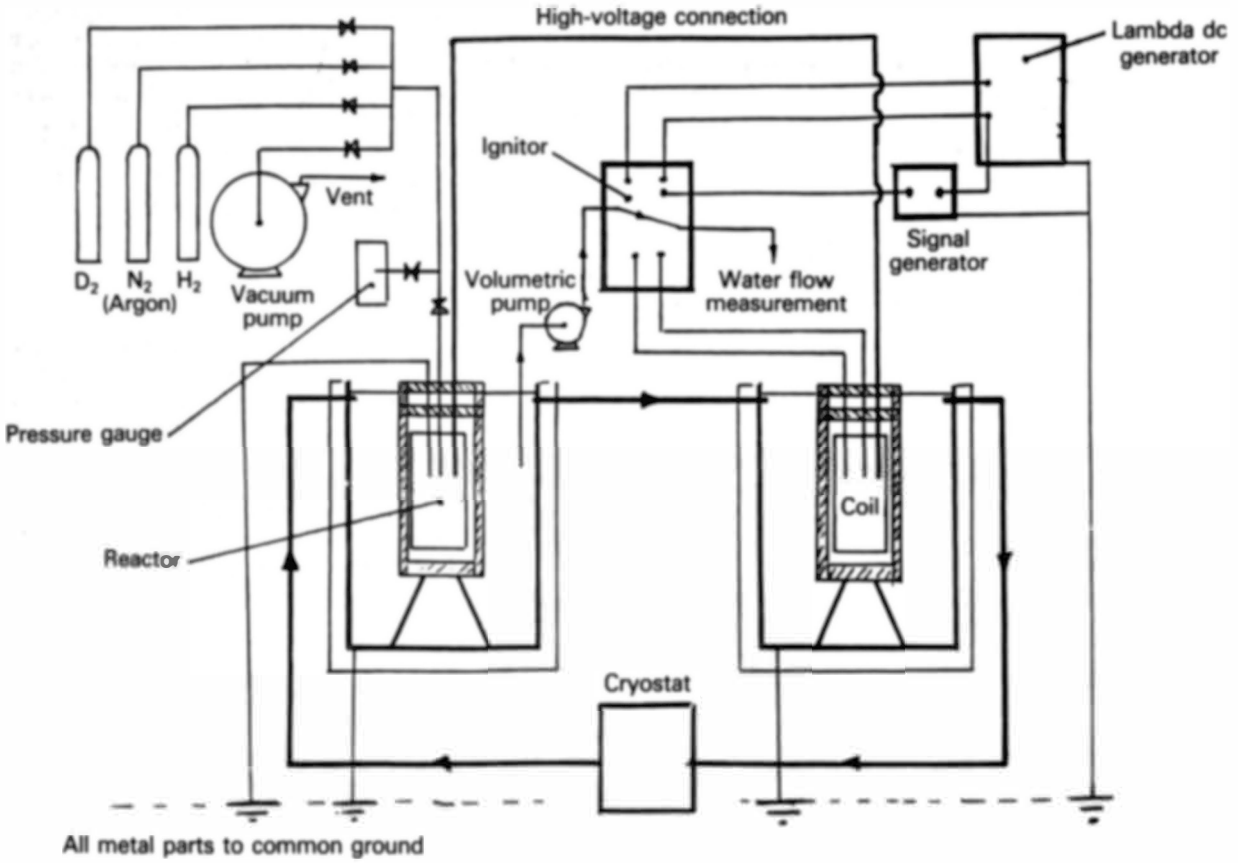

Fig. 2. Overall setup.

TABLE I

Gas Analysis

Argon (Matheson AG33)	Deuterium (Air Liquid N27)	Nitrogen (Quality U)	Hydrogen (Quality U)
Argon 99.9995%	$D^2/D_2 + H_2 \geq 99.7\%$	N_2 99.995%	H_2 99.995%
$H_2O < 2$ ppm	$H_2O \leq 2$ ppm $O_2 \leq 2$ ppm $N_2 \leq 2$ ppm	$H_2O \leq 5$ ppm $O_2 \leq 5$ ppm	$H_2O \leq 5$ ppm

capacitor through which the electrode is connected to ground) and several pointed electrodes (0.1-mm-diam copper wire; distance of tip to cylindrical electrode is 10 mm). The construction of the reactor makes it easy to change the cylindrical electrode to test various gas-metal combinations. Two metals were tested: palladium (Johnson-Matthey) and stainless steel.

The sparks are generated through a car ignition system comprising a coil (Valeo/Ducellier 2526021) and an electronic ignitor (Solex X.F1). The ignition system is powered by a stabilized direct current (dc) supply (Lambda 0/14 V), with tunable output voltage (see Fig. 3). The sparks are triggered by the action of a signal generator (Hewlett Packard HP 8111A).

The voltages and currents at various points of the system are monitored and recorded using two oscilloscopes (a Tektronix TK 5103 N and a Philips PM 3320 A). The dc low voltages and currents are also measured, using two digital hand-held multimeters (AOIP model MN5125C with current accuracy at 10-A range of ±0.3% and voltage accuracy of ±0.05%). These multimeters are used in the dc mode, in which they display mean values.

The heat released through the entire system is measured by three power meters as presented in Fig. 3. Two power meters are identical and static (see Fig. 4); they measure the heat released by the reactor and the coil. They are immersed in water (2 × 200-ℓ barrels; see Fig. 2) and are filled with dielectric oil, in which the reactor (or the coil) is immersed. The water temperature is maintained at 17°C by means of a Huber HS 40 cryostat. The third meter is dynamic and measures the heat released by the electronic ignitor (see Fig. 5). Various

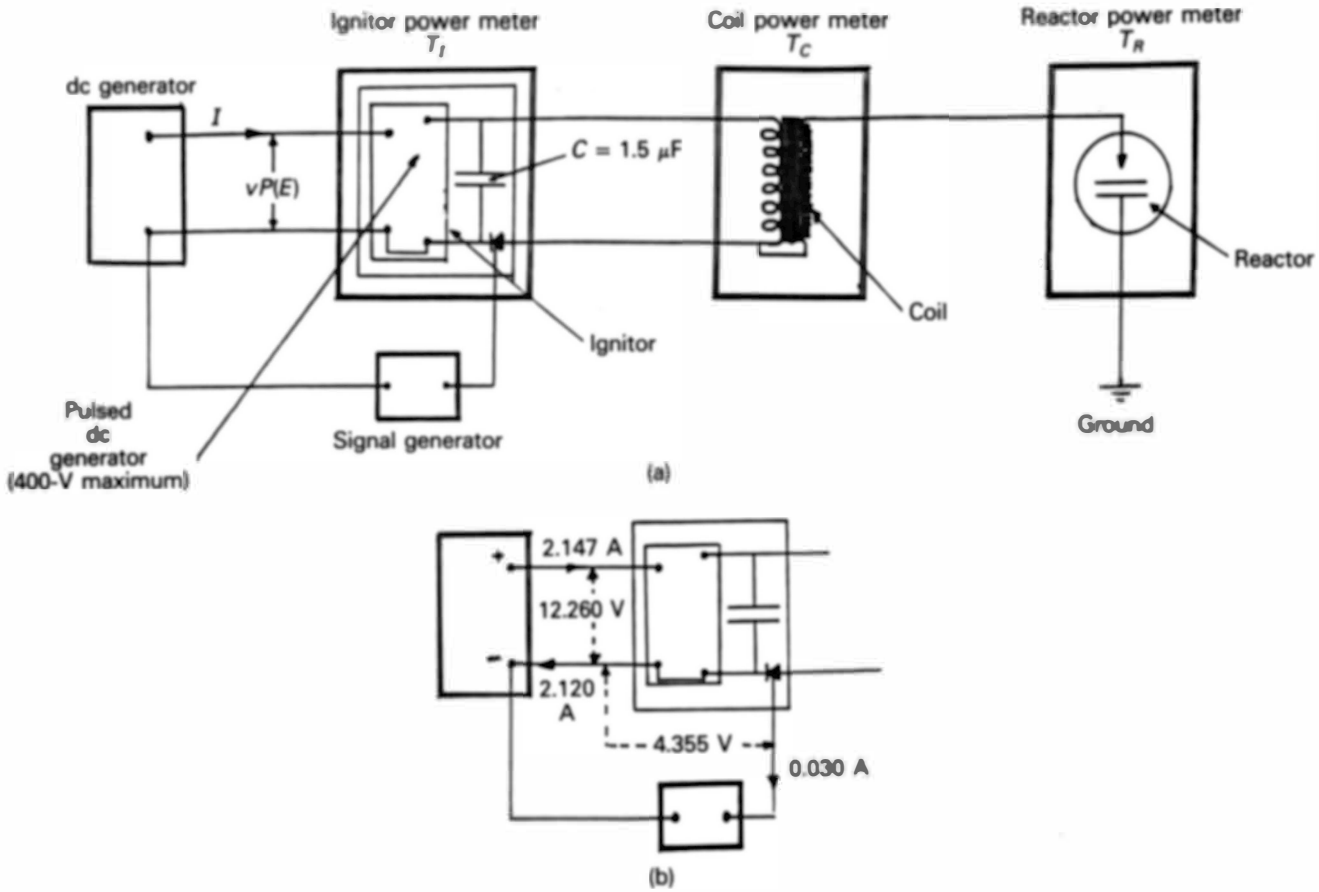

Fig. 3. Electrical supply and power balance.

temperatures (of the two static power meters and the ambient air) are measured using five temperature sensors [resistance temperature detector (RTD) type] connected to Eurotherm model 842 converters. Measurements are taken every 10 min and recorded. For the dynamic power meter, the temperatures are measured by high-precision mercury thermometers (1°C = 27 mm). Water flow is measured by using a gauge flask (500 cm^3) and a chronometer.

The entire installation is housed in an insulated portable cabin (4.0 × 2.5 × 2.3 m) placed in the shade. The internal temperature of the cabin is kept at a mean value of 21°C by the regulating action of a ventilation fan and an electrical radiator. The three power meters are installed in such a way that they receive no direct heat (or cold) from any source (sun, radiator, ventilation).

This setup enables a precise power balance of the whole system to be made, in accordance with the protocol that is described in the next sections. The overall installation is presented in Fig. 2.

IV. STRATEGY USED FOR THE POWER BALANCE OF THE SYSTEM

The four elements of the power balance of the system are summarized in Fig. 3. If we have

$P(E)$ = electrical power input

T_i = thermal power produced by the ignitor

T_c = thermal power produced by the coil

T_r = thermal power produced by the reactor

any excess energy $P(F)$ produced by the system will show up as a positive difference between the total thermal energy of the three power meters ($T_i + T_c + T_r$) and the electrical power input $P(E)$:

$$P(F) = T_i + T_c + T_r - P(E) \quad \text{(W)} . \tag{1}$$

In contrast, $P(F)$ should be zero when no excess energy is produced (with fluctuations around zero due to the noise in the measurements).

To identify such an excess of energy $P(F)$, the strategy was as follows:

1. Establish the calibration curves of the three power meters:

   a. For the two static power meters, the calibration gives the released power (T_c or T_r) as a function of a measured temperature difference.

   b. For the dynamic power meter, the calibration gives the released power T_i as a function of the measured power T_w carried away by the cooling water.

In order to take into account all possible small variations of the system during the course of the experiments (April to June 1991), calibration experiments were run before, during, and after the period.

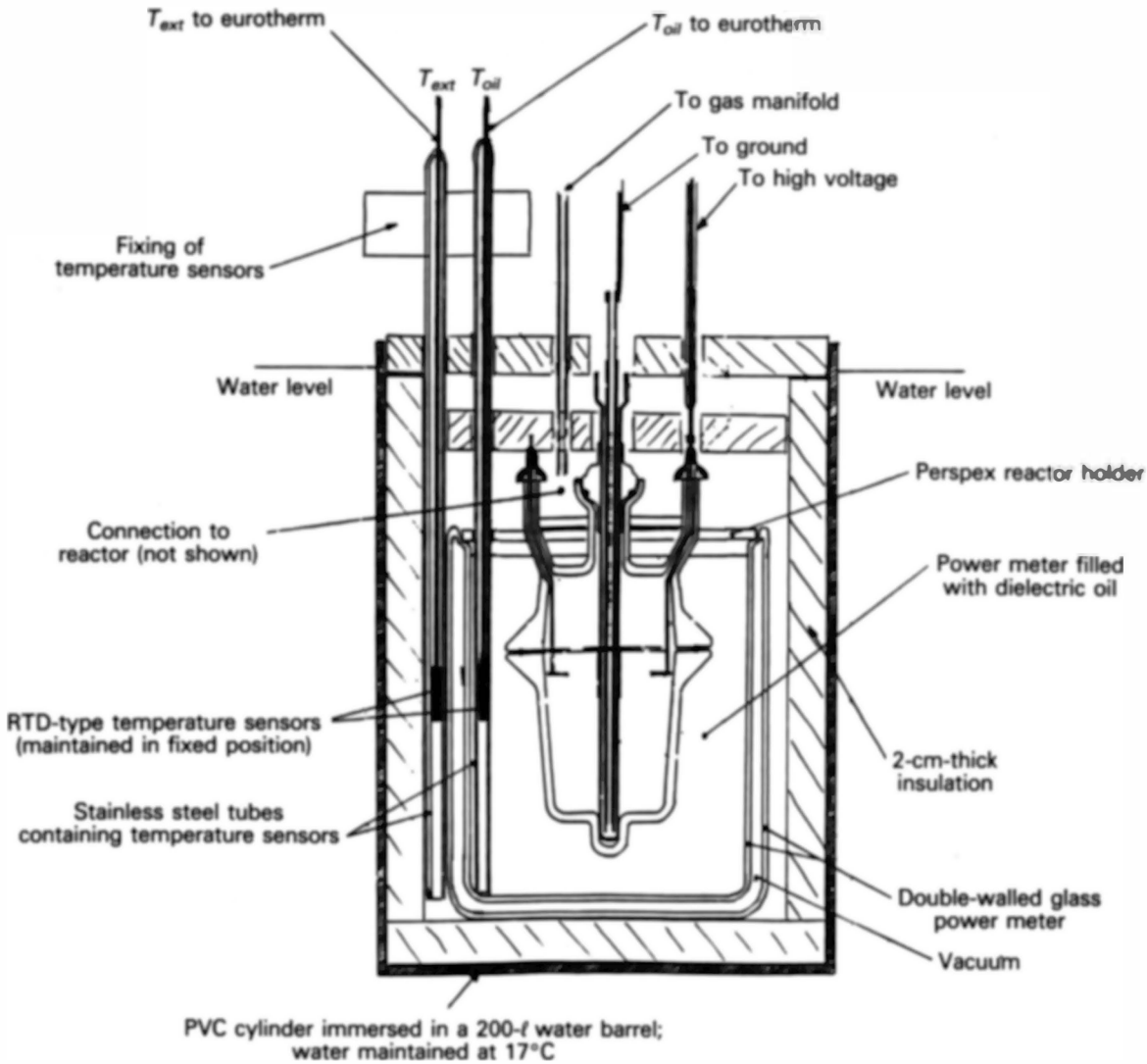

Fig. 4. Static power meters.

2. Measure precisely the electrical power input $P(E)$.

3. Use the three calibration curves obtained and the electrical power input to establish the power balance of three types of experiments:

a. "Reference" experiments were run in which heat is generated in the reactor by replacing the sparks by a resistance (heat is also generated in the coil and the ignitor through resistances). Twelve of these experiments were run, enabling the noise in the measurement of $P(F)$ to be determined. In this series, the mean value of $P(F)$ should be close to zero, yielding the baseline of the system.

b. "Active" experiments were then assessed against this baseline. In active experiments the reactor contains a hydrogen isotope, and sparking occurs between the electrodes. Seven active experiments (five with deuterium and two with hydrogen) were run in alternation with reference experiments.

It was carefully established that the thermal behavior of the reactor power meter was exactly the same in the reference and the active experiments and was not dependent on the way the power was delivered to the reactor.

c. "Control" experiments (three of them) were finally run. In the control experiments, the reactor is filled with a gas other than hydrogen isotope (argon and nitrogen were used), and sparking occurs in the reactor. They were also carried out in alternation with active and reference experiments (see Table II for the chronology of these experiments).

Measuring powers rather than energies has the great advantage that long-duration experiments can be run under steady-state and stabilized conditions, thus eliminating the effect of any transient phenomena occurring at the start of the process (such as hydride formation or action of traces of oxygen left in the reactor electrodes). Experiments with a duration from 48 to 1000 h have been run, each resulting in a perfectly stable and reproducible excess of energy production. This approach nevertheless presents a number of difficulties (influence of the position of the thermometers in the power meters, the thermal gradients built in, and the background

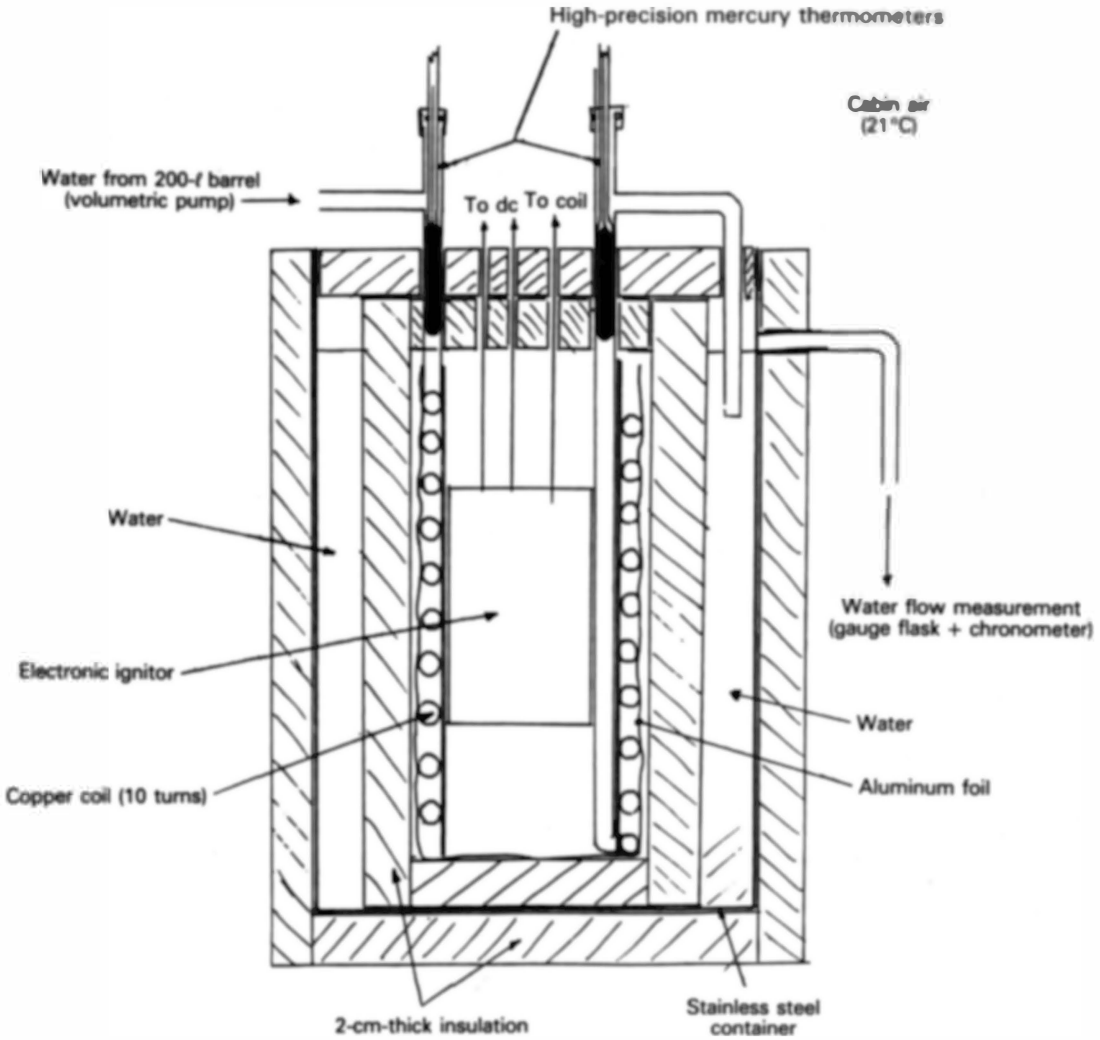

Fig. 5. Dynamic power meter.

temperature on the heat fluxes); these have been carefully taken into account as is explained later.

The detailed protocol for measuring the four elements of the power balances is described in Sec. V.

V. MEASURING THE ELEMENTS OF THE POWER BALANCE

V.A. Electrical Power In

V.A.1. Measurement of Electrical Power In

The ignitor consists of two parts: a pulsed dc current generator (maximum voltage 400 V) that charges a 1.5-μF capacitor connected to the coil primary, which discharges when triggered by the signal generator (through a thyristor valve). This discharge generates a high-voltage pulse in the coil secondary (see Fig. 3). Voltages and currents as a function of time are recorded using the Philips PM 3320A oscilloscope. Figure 6 gives the voltage and current shapes at the input of the ignitor system. The 2100-Hz pulses are produced by the electronics of the ignitor, as can be seen from the shape of the voltage at the coil primary (Fig. 7). Figure 8 gives the shape of the voltage at the coil secondary.

The AOIP multimeters were used to measure the mean intensity I of the current to the ignitor and the voltage difference V at the entrance of the ignitor (see Fig. 3). The electrical power in was thus calculated by

$$P(E) = V * I \quad (\mathrm{W}) \; . \tag{2}$$

From the shapes of the voltage and current curves as a function of time [$u(t)$ and $i(t)$] at the inlet of the ignitor (see Fig. 6), it was calculated that this value of $P(E)$ is systematically overestimated by some 0.5 to 1%. Since this results in a systematic underestimation of any excess of energy produced by the system, this measure of $P(E)$ was taken in the power balances.

At the end of the campaign, we compared $(V * I)$ with the mean value of the product $[i(t) * u(t)]$ as given by the PM 3320A oscilloscope. As can be seen from Table III, these measurements confirm the conservative value of $P(E)$ used in the power balances (overestimation by ~0.5 to 1%).

V.A.2. Possible Electromagnetic Interference Influence

Sparking in a gas between two electrodes creates currents that can be the source of voltage pulses in the surrounding grounded metal structures. Given the type of high-voltage

TABLE II

Power Balances

Date	Experiment[a]	Type	Gas-Metal Combination	Power Input (W)	Reactor Output (W)	Coil Output (W)	Ignitor Output (W)	Excess Energy Produced (W)
April 4	1	Type 1		22.23	5.67	6.69	10.3	0.43
April 10	2	Type 1		27.36	6.87	8.14	12.46	0.11
April 16	3	Type 1		15.71	4.19	5.24	6.84	0.56
April 23	4	Type 1		21.46	4.65	6.69	9.18	−0.94
May 2	5	Active	D_2/Pd	22.43	5.25	9.58	9.48	1.88
May 3	6	Type 2		25.05	3.92	13.73	7.24	−0.16
May 5	7	Type 2		32.34	6.63	14.31	11.14	−0.26
May 10	8	Active	D_2/Pd	30.91	6.42	12.83	13.57	1.91
May 13	9	Active	D_2/Pd	30.91	9.45	10.41	13.38	2.33
May 14	10	Active	D_2/Pd	31.04	9.71	10.06	13.24	1.97
May 16	11	Type 2		24.52	4.74	11.83	7.03	−0.92
May 20	12	Active	H_2/stainless steel	30.77	6.02	13.34	13.79	2.38
May 23	13	Type 2		19.57	14.89	2.03	3.21	0.56
May 28	14	Control	Argon/stainless steel	31.45	9.01	10.15	12.99	0.7
May 31	15	Type 1		19.88	11.91	8.42	−0.02	0.43
June 5	16	Control	Argon/stainless steel	29.99	4.01	13.91	12.99	0.92
June 9	17	Type 1		17.29	7.14	9.97	0	−0.18
June 12	18	Control	N_2/stainless steel	33.72	9.61	9.86	14.54	0.29
June 18	19	Type 2		12.15	4.33	8.23	0	0.41
June 26	20	Type 1		19.97	9.55	5.24	4.96	−0.22
July 1	21	Type 2		22.51	10.25	6.32	6.11	0.17
July 2	22	Active	D_2/stainless steel	25.55	5.64	10.71	11.04	1.84
July 4	23	Active	H_2/Pd	25.33	6.35	10.11	10.92	2.05

[a]In experiments 15, 17, and 19, the ignitor was not heated to check the zero of calorimeter 3.

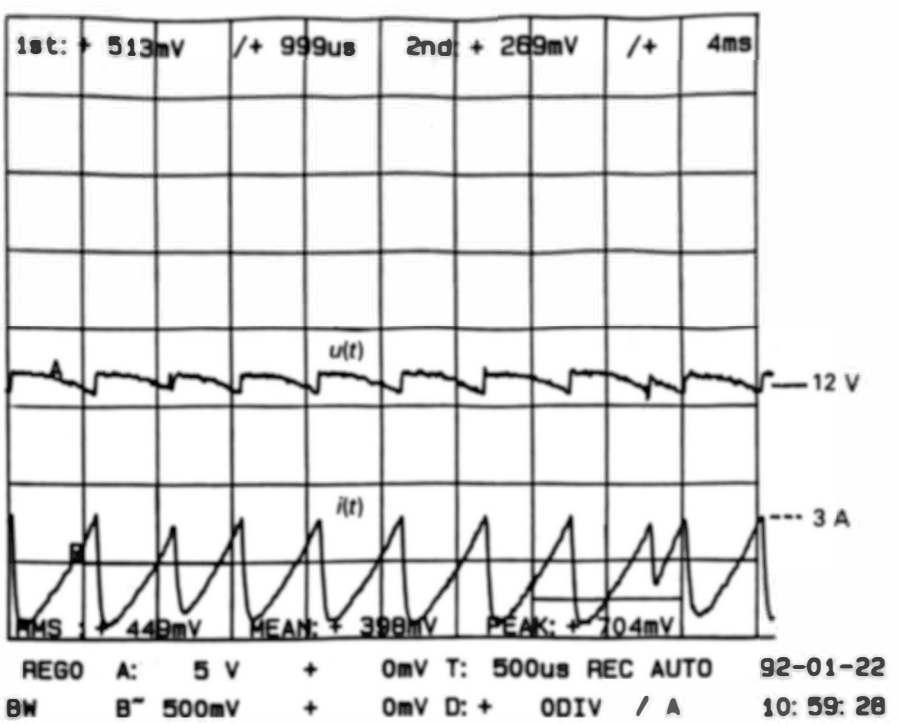

Fig. 6. Current and voltage at ignitor inlet

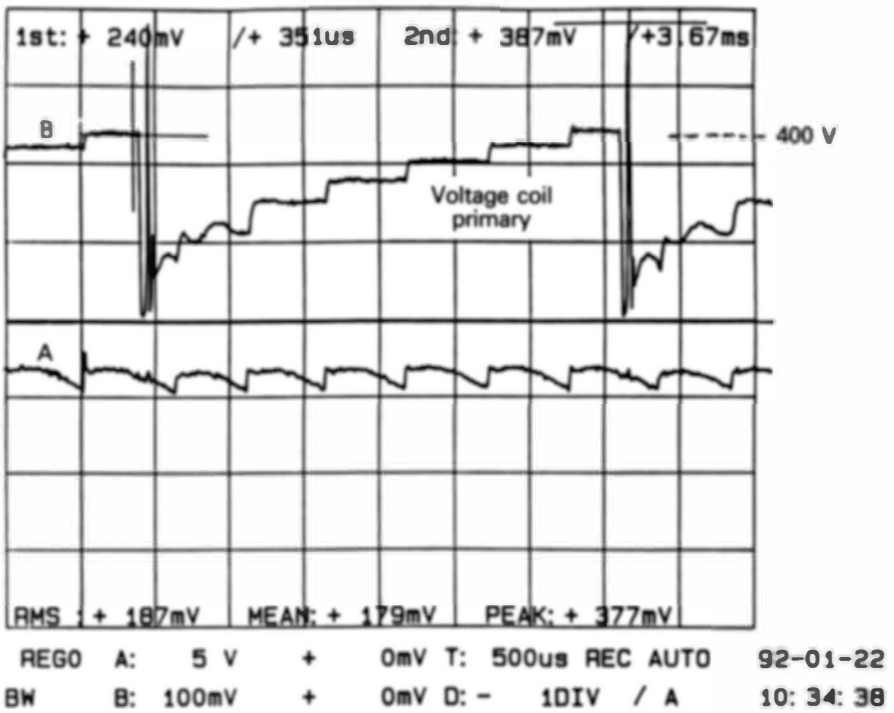

Fig. 7. Voltage at coil primary.

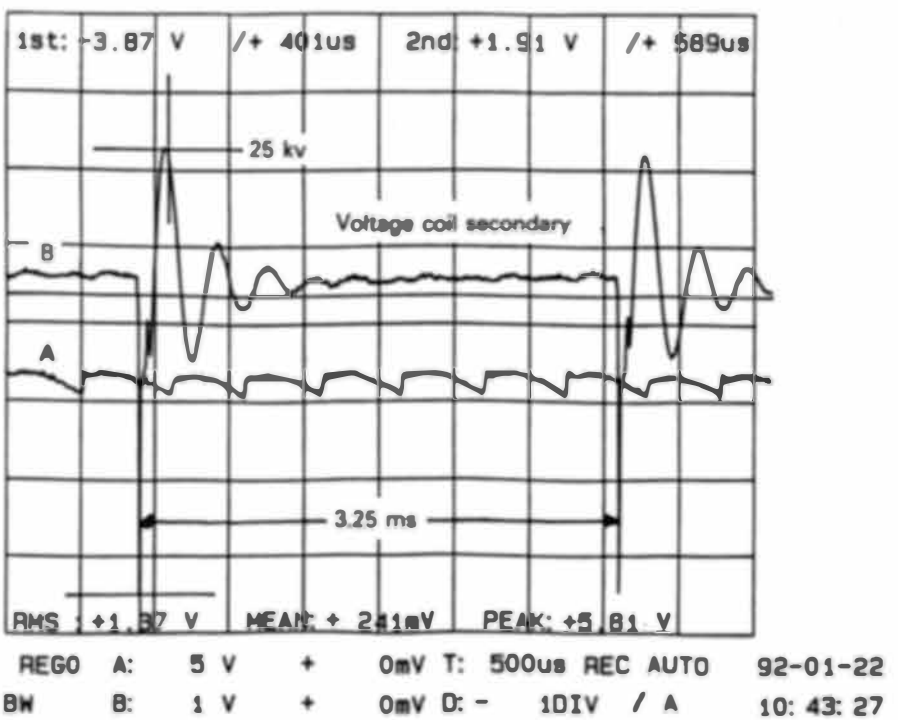

Fig. 8. Voltage at coil secondary.

generator used and the way it is connected to the dc generator (see Fig. 3), the net result of these currents is the underestimation of any excess of energy produced by the system. To check that the measure of $P(E)$ is not influenced by such factors, voltage and current balances were made on the lines connecting the dc generator to the electronic ignitor. Such a balance is shown in Fig. 3b; it excludes any unmeasured current flowing to the ignitor. Moreover, these balances show that the electrical power of the signals used to trigger the ignitor is negligible.

V.B. Thermal Power Produced by the Ignitor

V.B.1. Calibration of the Ignitor Power Meter

We refer to Fig. 5. To calibrate this dynamic power meter, a 2.5-Ω resistance was placed against the ignitor and heated by means of the dc generator (now delivering a constant dc current). The electrical input power was measured using the two AOIP multimeters. The thermal power released in the water flow T_w was obtained from the temperature difference of the water in and out [high-precision mercury thermometers (1°C = 27 mm mercury column) were used; see Fig. 5] and the water flow (chronometer and 500-cm^3 gauge flask). Typical values for the temperature difference was 0.3°C/W for a water flow value of 60 cm^3/min. At a power level of 12.5 W released by the ignitor, the standard deviation was 0.12 W. Ten sets of measurements were taken for each calibration point (over periods of 3 to 4 h and under fully stabilized conditions). Seven calibration points were obtained, yielding through linear regression the calibration curve of Fig. 9 (obtained for a mean background cabin temperature of 21.3°C):

$$T_i = T_w/0.7586 \ . \qquad (3)$$

At a power T_i of 12.5 W (which is the mean power used in our experiments), the temperature of the ignitor is ~55°C, thus enabling continuous operation with no damage to the electronics.

TABLE III

Comparison of Oscilloscope Measurements

AOIP			PM 3320A	
I (A)	V (V)	P (W)	$u(t) * i(t)$ (W)	Difference (W)
2.178	12.055	26.26	25.92	−0.34
1.880	12.163	22.87	22.73	−0.14
1.607	9.764	15.69	15.62	−0.07

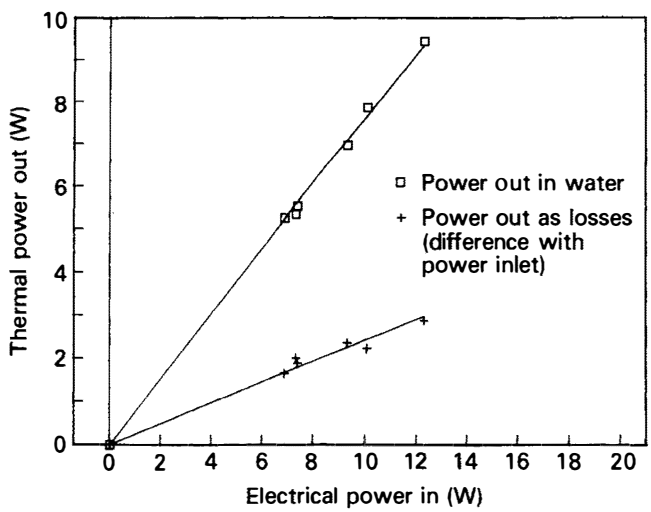

Fig. 9. Calibration curve for dynamic power meter.

V.B.2. Effect of the Background Temperature

As indicated in Fig. 5, the ignitor power meter is placed in the cabin. We have therefore quantified the effect of the temperature in the cabin (obviously, increasing the air temperature will increase the heat released to the cooling water). This was done by placing the power meter in a regulated oven, the temperature of which was varied between 20 and 35°C. By measuring the power T_w carried away by the water at two oven temperatures (25 and 35°C), it was found that, using Eq. (3), T_i was overestimated by 2 W (at a level of 12.5 W) when the air background temperature was 30.5°C (see Fig. 10). This quantification was not used to correct the calibration curve but to assess the possible effects of the (very slight) differences in background temperatures between calibration, reference, and active experiments, as is discussed later.

V.C. Thermal Power Produced by the Coil

V.C.1. Calibration of the Coil Power Meter

We refer to Fig. 5 (in which the reactor is replaced by the coil). The calibration curve of the coil power meter was obtained by heating the coil either by a resistance placed against it (calibration scheme 1: seven experiments) or by using the coil's own resistance (calibration scheme 2: five experiments), by passing a constant dc current through the resistance. The electrical power was measured by the AOIP multimeters, and the voltages were measured at the resistance terminals and current intensities in the line from the dc supply to the ignitor (see Figs. 11 and 12). The temperature difference $\Delta T = T_{oil} - T_{ext}$ (see Fig. 4) was measured on a fully stabilized system and was the result of 30 to 40 measurements taken each 10 min. Linear regression yielded the calibration curve of Fig. 13):

$$T_c = (\Delta T - 0.98) * 254.4/860 \quad (\mathrm{W}) \ . \qquad (4)$$

V.C.2. Controlling the Position of the Two Temperature Sensors

This key point was achieved by the special construction of the power meter (see Fig. 4), which enabled the coil to be manipulated between experiments, without losing control of this position. The coil was removed from the power meter and replaced several times, without any effect on calibration or reference experiments. Moreover, after all active and reference experiments, we checked whether the thermal gradients in the power meter were identical.

V.C.3. Effect of the Cabin Temperature

To assess the effect of the cabin temperature, we first stabilized the system at a cabin temperature of 35°C. At this temperature, T_{oil} and T_{ext} were measured, enabling T_c to be calculated [using Eq. (4)]. We then decreased the cabin temperature to 20°C and waited until the system was again stabilized (2 to 3 h). We then measured T_{oil} and T_{ext}; we found that T_{oil} had decreased by ~0.5°C and that T_{ext} had not varied. The new value of T_c given by Eq. (4) is then 0.15 W lower than that found for a cabin temperature of 35°C. From this we conclude that the influence of the cabin temperature on the value of T_c is negligible.

V.D. Thermal Power Produced by the Reactor

The thermal power produced by the reactor is measured in a similar way, the reactor being heated by a resistance

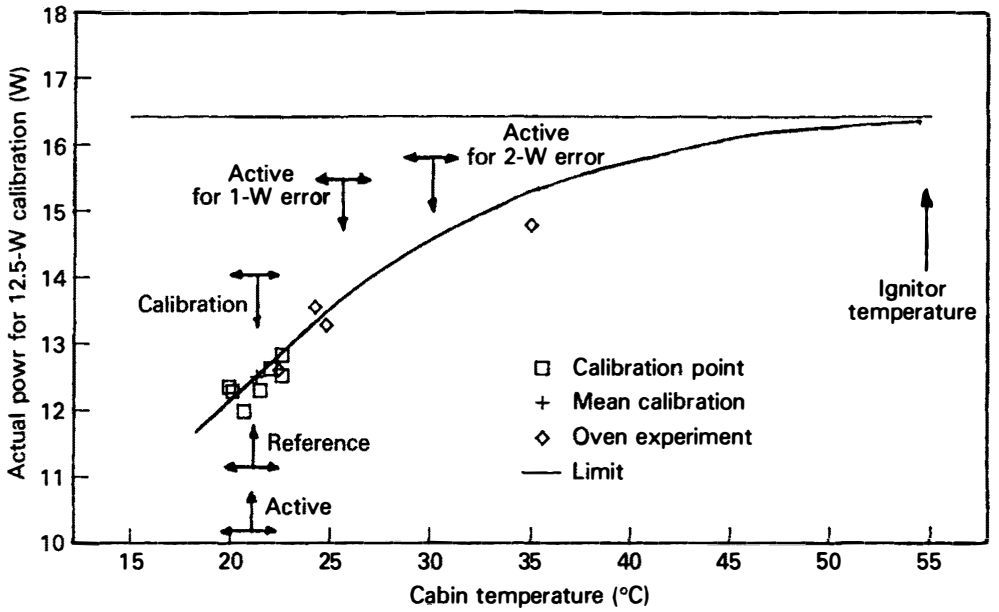

Fig. 10. Influence of cabin temperature on dynamic power meter.

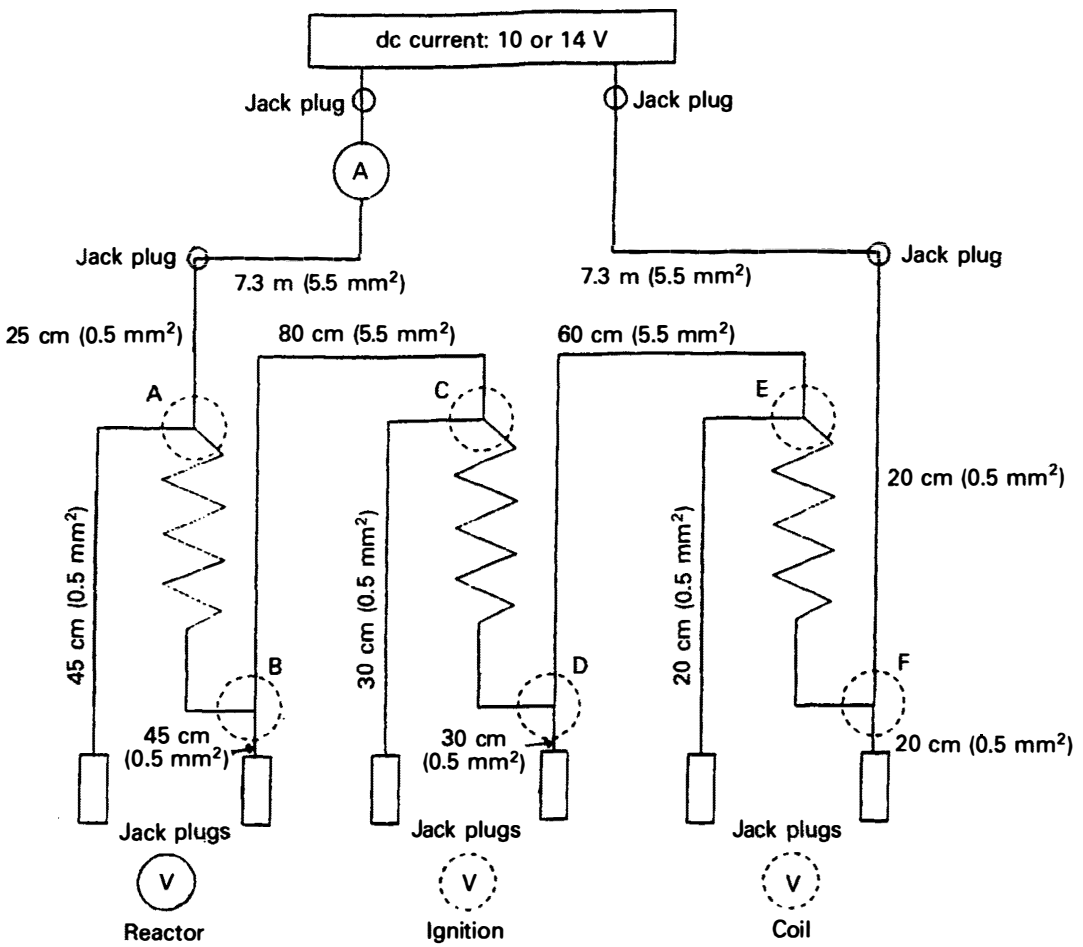

Fig. 11. Calibration scheme 1: three electrical resistances.

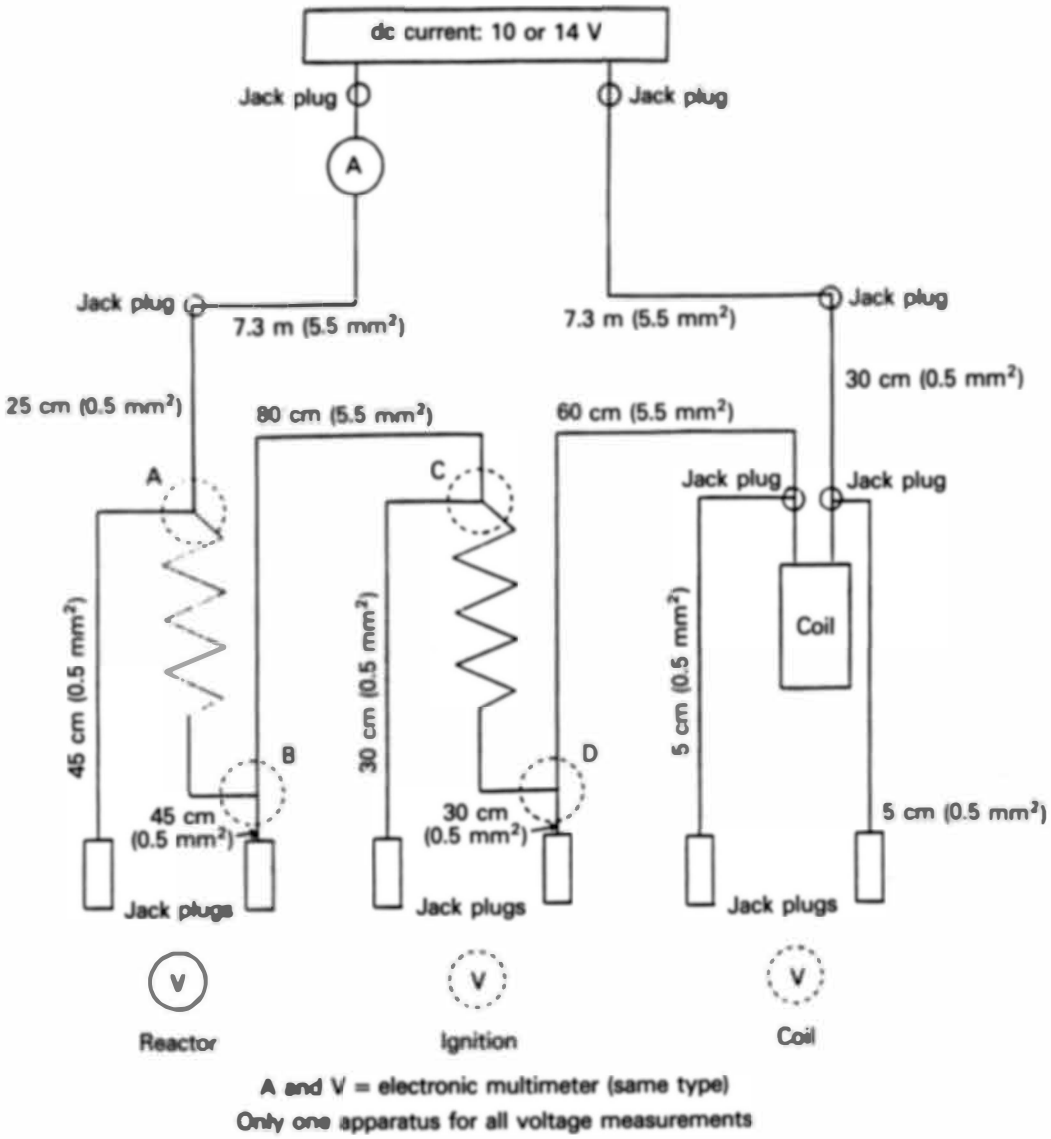

Fig. 12. Calibration scheme 2: two electrical resistances and coil as a resistance.

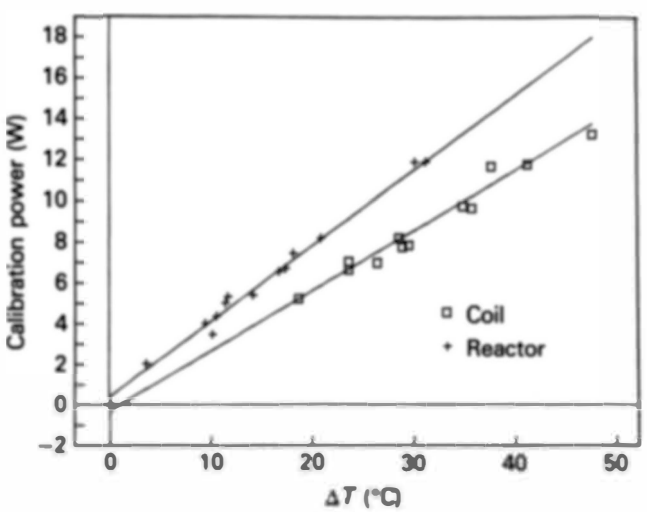

Fig. 13. Calibration curve (coil and reactor).

placed against the cylindrical electrode. The calibration curve obtained from 13 experiments is (see Fig. 13)

$$T_r = (\Delta T + 1.1) * 319.9/860 \quad (\mathrm{W}) . \qquad (5)$$

The observed difference in the heat transfer coefficient is due to the different shapes of the reactor and the coil (the coil is completely immersed in the oil of the power meter, whereas a small part of the reactor is not). As was the case for the coil, the reactor was removed and replaced in the power meter with no influence on the calibration and reference experiments. No influence of cabin temperature change was observed on the value of T_r.

VI. NET HEAT RELEASE WITH HYDROGEN ISOTOPES

VI.A. Measurement of the Excess Energy Production

The excess energy production was measured during a campaign that lasted from April 4 to July 3, 1991. Thirteen

reference, seven active, and three control experiments were run in the sequence given in Table II. Of the reference experiments, eight were run when heating the system through resistances (reference type 1), and five were run when heating the coil through the ignitor and with a resistance in the reactor (reference type 2) (see Figs. 14 and 15). Of the seven active experiments, four were run with a combination of deuterium and palladium, one with a combination of deuterium and stainless steel, one with a combination of hydrogen and palladium, and one with a combination of hydrogen and stainless steel.

A new electrode was used for each experiment with stainless steel. The same virgin palladium electrode was used for the entire period. This electrode was degassed (vacuum, 150°C) on May 3 and 24, 1991.

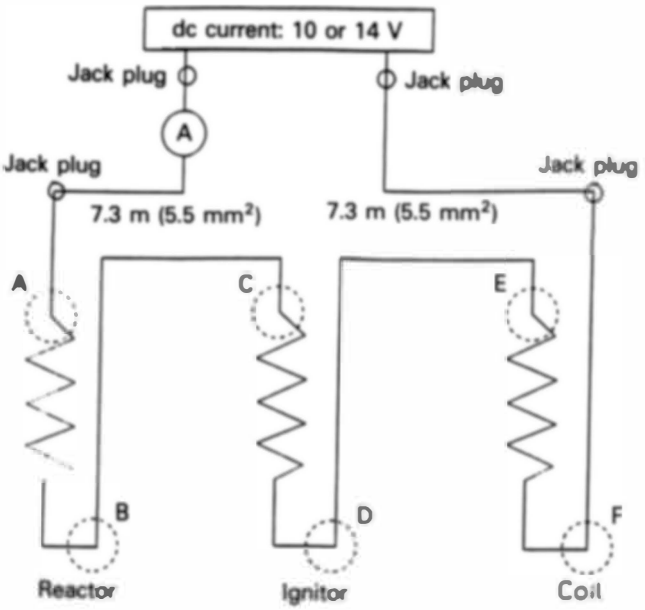

Fig. 14. Reference experiment type 1: three electrical resistances.

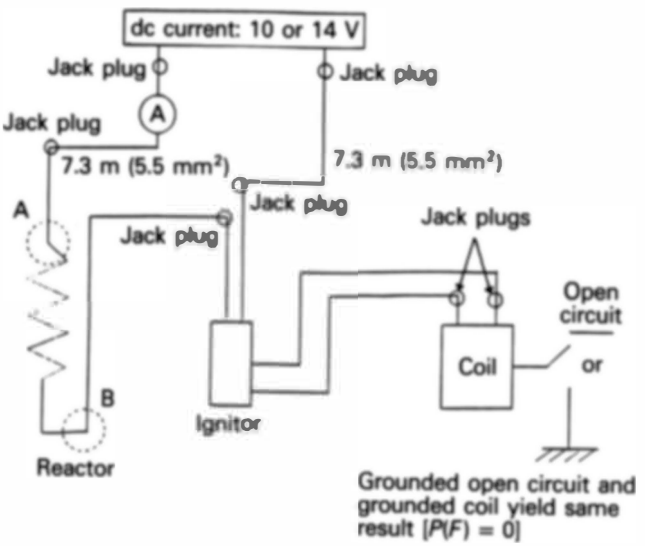

Fig. 15. Reference experiment type 2: one electrical resistance, ignitor in line, and coil.

Two control experiments were run with a combination of argon and stainless steel and one with nitrogen and stainless steel. Table II summarizes the conditions of these experiments, which were collected after stabilization of all the temperatures of the system (10 to 48 h depending on the amplitude of the changes in these temperatures) and complete loading of the electrode with the hydrogen isotope (24 h when starting from a degassed cathode). It is thus impossible to say exactly when the excess energy production starts, but it is at maximum 48 h after starting an experiment with a degassed electrode.

The degree of the charging of the electrode with hydrogen isotope was measured from the pressure variations of the reactor during the initial loading period, ending when the pressure is stabilized (taking into account the necessary makeup of the isotope). Preliminary tests had shown this procedure to be correct: Degassing a loaded electrode (200°C, atmospheric pressure) resulted in a 95% recovery of the hydrogen isotope.

All the measurements obtained in accordance with the protocol were used to establish the power balances of all experiments, using the calibration curves given by Eqs. (3), (4), and (5). The elements for these power balances are given in Table II.

The excess energy production $P(F)$ for these various experiments is plotted chronologically in Fig. 16. The following can be seen:

1. All excess energy production measurements in the reference experiments fall around zero (mean value 0 W, standard deviation 0.49).

2. All active experiments show excess energy production of ~2 W (mean value 2 W, standard deviation 0.21).

3. The three control experiments fall within the 95% confidence level of the reference experiments, on the high side but out of the 95% confidence level of the active experiments. The mean value of the excess energy for these control experiments is 0.63 W. The deviation from the baseline is likely due to the lower number of control experiments compared with that of the reference experiments.

The maximum duration of excess energy production during this series of experiments was 216 h (450 W/h produced).

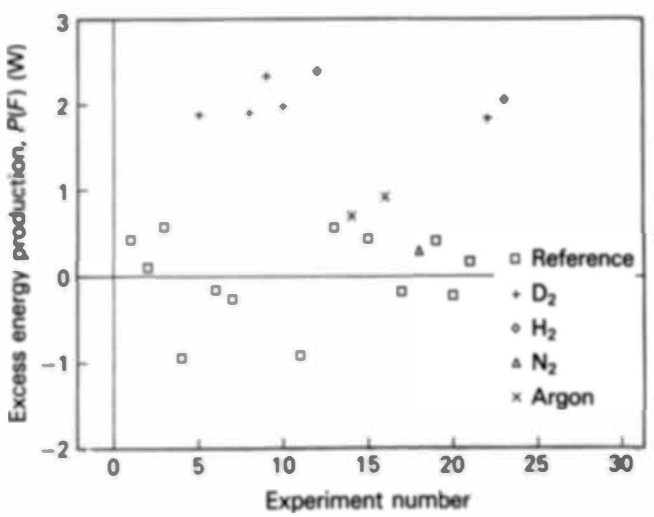

Fig. 16. Reference and active experiments: excess energy production.

A 1000-h experiment was run in a search for tritium and is reported in Sec. VII.A.2. So far, all experiments have been stopped before any indication of a decrease in the excess energy production.

VI.B. Effect of the Way the System is Heated

During the calibration of the various parts of the system, we used heating resistances. One may wonder whether this is representative of the situation in active experiments. The answer is clearly "yes" for the coil and the ignitor: Five reference experiments type 2, as shown in Fig. 15 (Table II, experiments 6, 7, 11, 13, and 21), fall within the losses of other reference experiments.

The case of the reactor remains to be examined. To check that its thermal behavior was indeed the same during the active and the reference experiments, we have plotted the two temperatures used in calculating the ΔT, as a function of ΔT. The results are plotted in Fig. 17 (Fig. 18 gives a similar plot for the coil). We have also compared the thermal gradient in the oil of the power meter for the two types of experiments by measuring, at the end of each one (after cutoff of the power for safety reasons), the temperatures at various levels in the power meter. The temperatures for two of these levels (bottom and +8 cm from bottom) are plotted as a function of the ΔT of the power meter in Fig. 19 (Fig. 20 gives a similar plot for the coil).

From these data, it can be concluded that the thermal behavior of the reactor (and the coil) is exactly the same in the active and the reference experiments, all experimental points being on the same correlation. Heating the reactor with a resistance in the reference experiments thus introduces no systematic difference from the situation of the active experiments. (Note that the reactor power meter works in the stratified regime and the coil power meter works in the mixed regime, which is in line with the respective shapes of the reactor and the coil.)

In addition, three control experiments run with nitrogen and argon to check this point fall within the range of the reference experiments.

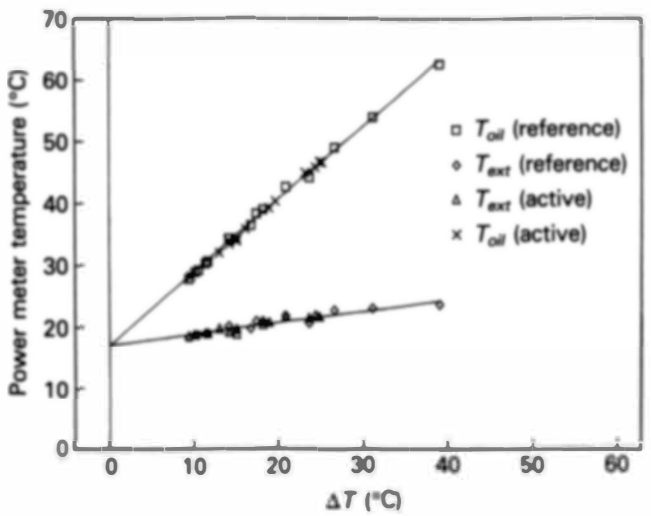

Fig. 17. Reactor temperature as a function of ΔT.

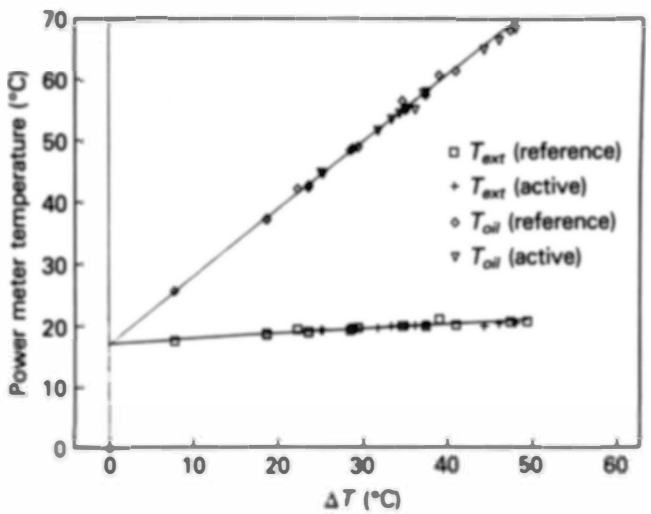

Fig. 18. Coil temperature as a function of ΔT.

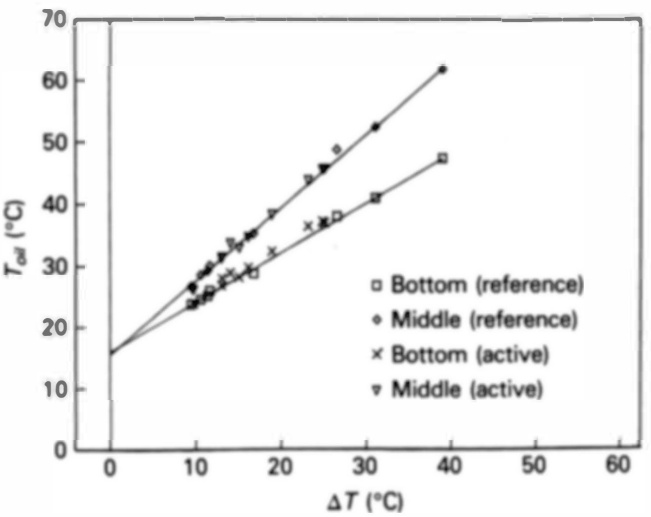

Fig. 19. Reactor thermal gradient.

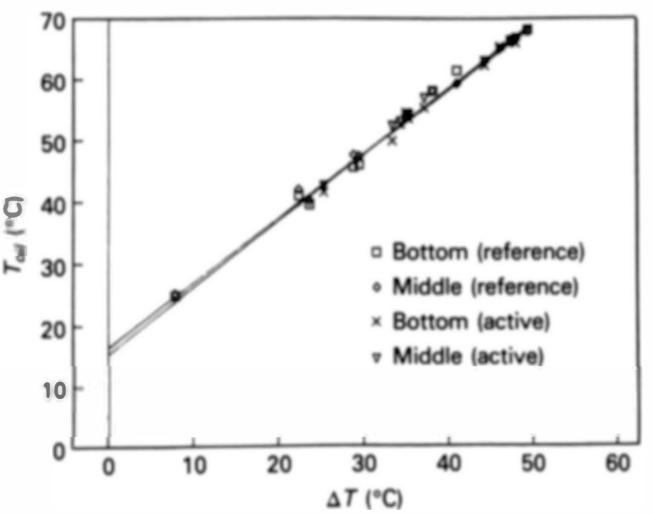

Fig. 20. Coil thermal gradient.

VI.C. Effect of the Cabin Temperature

We have seen that a variation of the cabin temperature (between 21 and 35°C) has a negligible effect on the amount of thermal power released by the coil and the reactor. On the contrary, a variation of this temperature from 21 to 30.5°C would cause an overestimation by 2 W of the heat released by the ignitor (see Fig. 10). This would explain the excess energy production observed, if the change of cabin temperature were from 21°C for the reference and control experiments to 30.5°C for the active experiments. The actual values for these temperatures are as follows (mean values and range):

1. reference experiments: 21.1 ± 1.5°C
2. control experiments: 20.7 ± 0.7°C
3. active experiments: 21.3 ± 1.6°C.

From these data, it is concluded that the thermal conditions in the cabin were essentially the same during all the experiments (which is not surprising owing to the random sequence of the various experiments).

Thus, cabin temperature variations cannot explain the net heat release measured during active experiments.

VI.D. Effect of the Contact Resistances

During the course of the experiments, a number of electrical connections have to be plugged in and taken out. This may lead to uncontrolled contact resistances. To check this, the voltage drops in the circuit were recorded, and the average value for each experiment have been plotted against the current (see Fig. 21, in which the voltage drop in the mains is the drop in the lines between the dc supply and the ignitor and the drop in the secondary is in the lines between the resistances). As can be seen in Fig. 21, the voltage drops in the mains are in line for the reference and active experiments, and the voltage drops in the secondary are negligible for the calibration experiments. Contact resistances thus have no influence on the power balances.

VI.E. Net Heat Release with Hydrogen Isotopes

The conclusion drawn from this series of experiments is that a net energy production $P(F)$ of ~2 W is generated when hydrogen or deuterium is subjected to sparking between two electrodes. Excess energy during the electrolysis of light water has already been observed.[23] The excess energy production occurs for two different electrode metals: palladium and stainless steel. It is likely that it would also occur with other metallic hydride-forming metals.

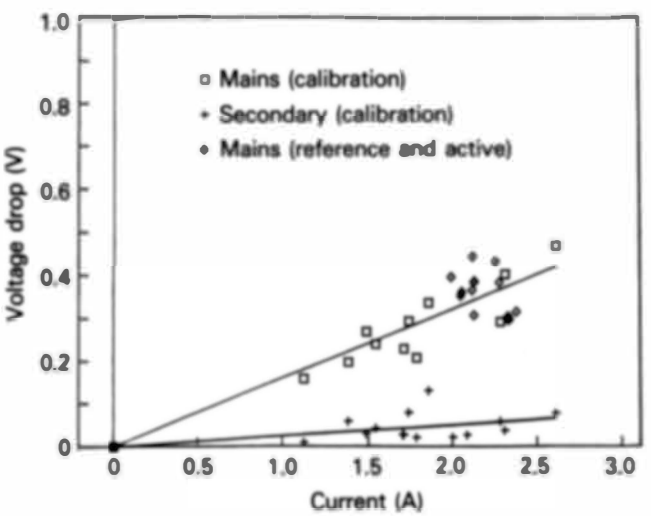

Fig. 21. Contact resistances.

Of great interest is the detailed examination of the evolution of the total energy released in the reactor in experiments 8, 9, and 10, which were run without any change in the system for a total period of 216 h. This energy increases from 6.42 W at the beginning to 9.71 W at the end of the period. We attribute this increase to the progressive buildup of ionizing species in the gaseous gap between the electrodes, diffusing from the electrode to the gas (β^- emitters, see Sec. VIII.C). These ionizing species reduce the electrical resistance of the gas, resulting in more electrical energy being released in the reactor (and less in the coil, because the total electrical energy delivered to the coil-reactor system remains constant). On the contrary, the excess energy production remains essentially constant during the period (mean value 2.1 W, standard deviation 0.2 W). This clearly indicates that the excess energy is governed by phenomena occurring at the impact of the sparks on the electrode and not by the action of the sparks in the gas. Reducing the electrical energy deposited in the gas (shorter sparks at same frequency) will thus result in an increase of the efficiency of the process.

That the electrical energy released in the reactor depends on the electrical properties of the gas (breakdown voltage, ion mobilities, attachment, etc.) is clearly shown in control experiments 14 (argon) and 18 (nitrogen), where the total energy released in the reactor is ~9 W. At this level, the deviations from the baseline are 0.7 and 0.29 W, within the 95% confidence level of the baseline. To check any influence of the level of the electrical power deposited in the reactor, experiment 16 (argon) was run with a slightly increased distance between the electrodes (12 mm instead of the 10 mm for all the other experiments), reducing the frequency of the sparks, thus resulting in less electrical energy being deposited in the reactor (4 W). The deviation from the baseline was 0.92 W, still within the 95% confidence level of the baseline. Thus, the variations of the electrical energy deposited in the reactor cannot explain the results of the experiments with hydrogen isotopes.

No systematic deviation can thus be found in the measurements that could explain the statistically significant differences observed among the reference, active, and control experiments. Calculation of the maximum heat release that could be due to complete combustion of the hydrogen isotope in the reactor, combined with analysis of the reactor gas phase after the experiments (only very small amounts of nitrogen and argon were found) completely excludes the heat of oxidation as an explanation (for the 1000-h run, the difference is five orders of magnitude). The very stable excess energy production, observed over periods of >48 h, also excludes any transient exothermic reaction.

We thus have to look for another explanation, which is likely to be nuclear and probably nonclassical. Such a hypothesis is given in Sec. VIII. We first report on searches for signs of a nuclear reaction, the first one carried out (for safety reasons) before the excess of energy production measurement campaign of April–July 1990 and the second performed in June–July 1992 with a specific device.

VII. EMISSION OF RADIATION

Before running experiments to measure precisely the excess energy production in our system, we initially assessed

whether there was any emission of radiation (for safety reasons). This assessment was performed in October–November 1989. A second assessment was performed in June–July 1992 with a detection system better adapted to cold fusion triggered by sparking. The results of both assessments are now reported.

VII.A. October–November 1989 Assessment

VII.A.1. Detection Devices Installed

The three known fusion reactions involving deuterium were monitored:

$$D + D = {}^3He\ (0.8\ MeV) + n\ (2.5\ MeV)\ (50\%) \quad (6)$$

$$D + D = T\ (1.0\ MeV) + p\ (3\ MeV)\ (50\%) \quad (7)$$

and

$$D + D = {}^4He + \text{gamma photon}\ (23.8\ MeV)\ (10^{-4})\ . \quad (8)$$

Radiation measurements were performed using two types of devices (active and passive) for neutrons, gamma and X-ray photons, and charged particles. Liquid-scintillation counting was used for tritium detection. Various metal-hydrogen combinations were assessed, as indicated with the results.

VII.A.1.a. Active detection devices: The following active detection devices were used:

1. A neutron detector, using a ^3He proportional counter and a multichannel analyzer (MCA) was used. This technique gives no information on the energy of the detected neutrons.

2. A gamma photon detector was also used that was based on a sodium iodide (thallium-activated form) scintillation counter (6.62-cm-long × 3.81-cm-radius cylindrical sodium iodide crystal). The pulses were analyzed by an MCA.

As expected, these devices were very sensitive to perturbations caused by sparking in the reactor, thus rendering the spectra obtained with the MCA unusable. We thus used passive devices, which are insensitive to these perturbations.

VII.A.1.b. Passive detection devices: The following passive detection devices were used:

1. Neutron detection by activation analysis was tried, using gold, indium, dysprosium, and europium. The gamma spectra of the (possibly) activated products were recorded with the aid of a high-purity germanium detector (in a location free from electrical disturbances).

2. Neutron detection was also performed by track etching using a track-etching film covered with boron. The sensitivity of this type of detector is estimated to be 2×10^{-4} n/s·cm^2.

3. Gamma and X-ray photons and charged particles were detected with the aid of an X-ray film (Agfa-Gevaert/Structurix D7+Pb). These films are delivered by the manufacturer with two thin layers of lead (27 μm) covering both sides of the film, inside a light-tight envelope. This increases the sensitivity of photon detection. We added additional layers of lead to all the films (outside the light-tight envelope) to create a scale that could provide some information on the energy of the impinging photons or on the range and energy in the case of charged particles (X-ray film covered by one to five layers of 27-μm lead). In each experiment aimed at measuring emissions, a layered film was placed inside the reactor, at the upper part and against the wall, and a second one was placed outside the reactor, in the lower part and against the wall (4-mm-thick wall) (see Fig. 22 for this setup).

Alternatively, radiation detection with X-ray film was carried out using highly sensitive dental films (Emmenix). These films are covered by a 250-μm layer of lead containing plastic. Four of these films were placed in the reactor, two against the wall and two around the 10-mm tube supporting the metal being tested (at more than 2 cm of the impacts of the sparks). A number of experiments have been run with this setup, both with hydrogen and deuterium.

4. We attempted to detect tritium after a 1000-h run carried out with one reactor placed in one of the static power meters (deuterium-palladium combination) while a second reactor was run in parallel in the second power meter (nitrogen-stainless steel combination). This enabled relative energy balances to be made during the run; an excess energy production of 2 W was found in the deuterium-palladium experiment. After the end of the run, the nitrogen and argon contents of the (deuterium) reactor gas phase were measured by chromatography (1% N_2, 85 ppm argon), and the remains of the gaseous phase of the reactor were transferred in an intermediate stainless steel storage vessel under pressure. The palladium electrode (now filled with deuterium) was transferred to a specially designed oxidation reactor. After the oxidation reactor had been emptied under a vacuum of 10 mm mercury, the gas phase of the reactor was transferred into it.

The oxidation reactor was then heated to 350°C, which resulted in deuterium release from the palladium electrode (which was traced by the pressure variation). The content of the reactor was then oxidized (N27 oxygen), and the resulting heavy water was recovered. The overall operation resulted in recovery of 80% of the deuterium introduced into the reactor during the 1000-h run. Air entry (measured by chromatography of the residual oxygen after oxidation) was <2% of the total reactor gas phase. The tritium content of the recovered heavy water was determined by liquid-scintillation counting. A blank experiment was run using the same procedure but with deuterium from the gas bottle.

VII.A.2. Result of the Radiation Measurements

VII.A.2.a. Active devices: As stated earlier, electrical perturbations caused by the sparks prevented the use of the spectra obtained with the active devices.

VII.A.2.b. Passive devices: Neutron detection by activation analysis did not yield any results: No gamma-ray emission was detected after activation.

VII.A.3. Neutron Detection by Track Etching

The results are summarized in Table IV. The sensitivity of this type of detector is estimated to be 2×10^{-4} n/s·cm^2.

TABLE IV

Neutron Detection Results

Experiment	Response (n/s·cm^2)	96% Confidence
Background (1)	9×10^{-5}	$5 \times 10^{-5}/1.3 \times 10^{-4}$
Hydrogen-palladium (2)	9×10^{-4}	$3 \times 10^{-4}/1.5 \times 10^{-3}$
Deuterium-palladium (3)	4×10^{-4}	$1 \times 10^{-4}/7 \times 10^{-4}$

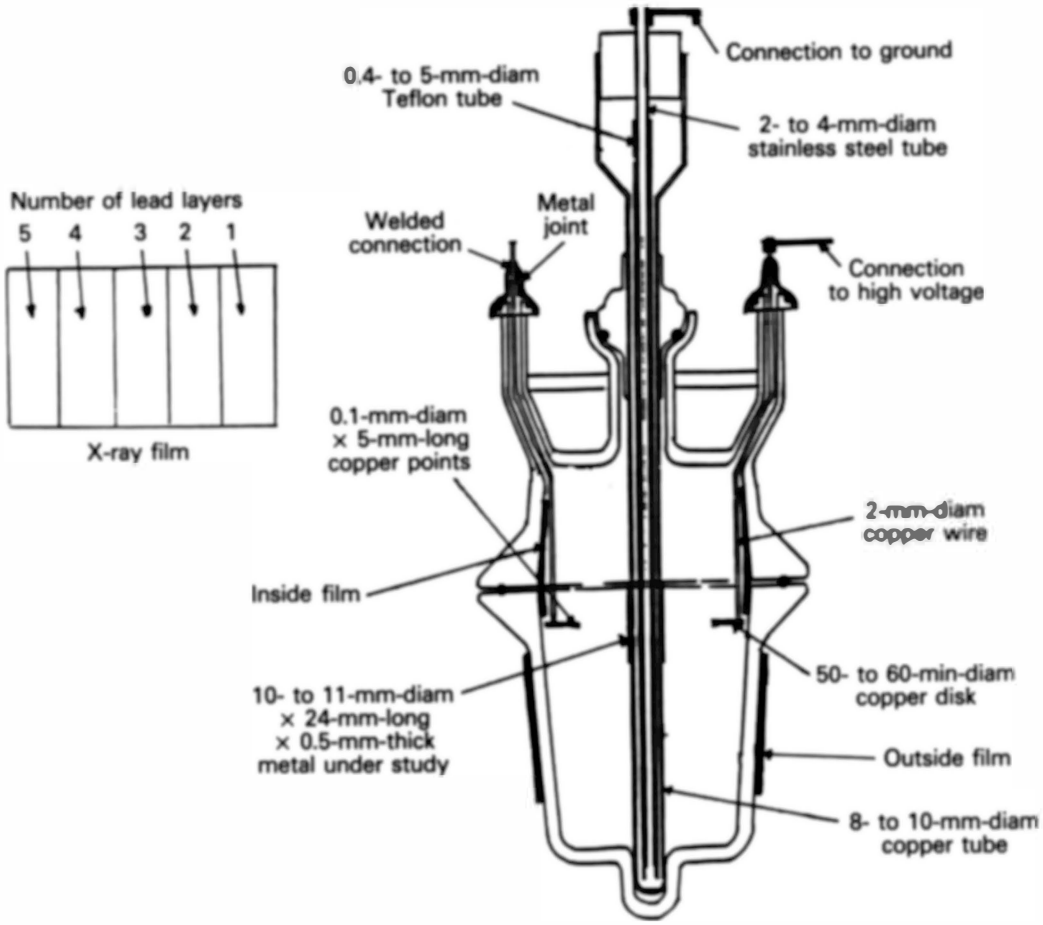

Fig. 22. Film setup.

The values suggests a somewhat higher response than background for both experiments 2 and 3. If we assume that no nuclear reaction occurs with hydrogen, the similar response for experiments 2 and 3 suggests that this response is most likely not due to neutrons and that the background may be somewhat higher in the reaction vessel. Since we are looking for a nonclassical reaction, we have an upper limit for the neutron emission (film placed at 35 cm from the source):

1. 12 n/s in the case of a hydrogen-palladium system
2. 4.5 n/s in the case of a deuterium-palladium system.

This last value is many orders of magnitude lower than what would be expected from fusion reaction (6): 4×10^2.

Tritium detection by scintillation gave the results listed in Table V. These values suggest that the amount of tritium in the water from the reactor does not increase. However, the very low level of one sample of the blank experiment is puzzling. The result could be due to the procedure used: for both deuterium-palladium and blank experiments, the reactor was flushed twice with ordinary water, and the resulting samples (6, 6b, 14, and 15) were not mixed. To have an upper limit for the amount of tritium that could have been formed during the 1000-h run, we have considered the highest value of the deuterium-palladium experiment and the lowest of the blank experiment. We find tritium $<4 \times 10^9$. This value is again many orders of magnitude smaller than what would be expected from fusion reaction (7): 1×10^{19}.

TABLE V

Tritium Detection Results

Experiment	Tritium Level (Bq/cm^3)
Deuterium-palladium (sample 6)	0.2
Deuterium-palladium (sample 6b)	0.16
Blank (sample 14)	0.02
Blank (sample 15)	0.16

The results obtained for gamma and X-ray photons and charged particles with the X-ray films placed as indicated in Fig. 23 are listed in Table VI.

As for the experiments run with the Emmenix dental films, following results were obtained:

1. Under similar conditions of activation, film blackening was stronger with deuterium than with hydrogen. Little or no blackening was observed with nitrogen.

2. The films around the tube supporting the metal under study were in all case more blackened than the films against the wall inside the reactor.

3. The films outside the reactor were not blackened.

TABLE VI

Photon and Charged-Particle Results

Position	Experiment	Blackening
Inside reactor	N_2-stainless steel	Very slight
Outside reactor	N_2-stainless steel	No
Inside reactor	Deuterium-palladium	Strong and uniform
Outside reactor	Deuterium-palladium	No
Office	Background	No

We attribute the very slight blackening observed with nitrogen to very small amounts of X-rays generated by the high-energy tail of the electrons in the discharge. As regards the strong blackening observed with deuterium (and hydrogen) we eliminate three possible causes:

1. Light or ultraviolet radiation cannot have any effect on the light-tight films used.

2. Molecular hydrogen is likely to be able to diffuse in small quantities through the envelope holding the films but cannot reduce the silver salts of the emulsion at the reactor temperature (maximum 40°C).

3. Atomic hydrogen, which could reduce the silver salts, cannot go through 250 μm of plastic without recombining. Calculations based on the kinetics of this recombination show a maximum depth of penetration of some 20 to 30 Å.

We thus explain this blackening by the action of ionizing radiation, which can be alpha particles, beta rays, or low-energy X-rays. The striking difference between the films inside and outside the reactor in the deuterium-palladium experiment can most likely be explained by the emission of charged particles, very probably electrons of fairly low energy (~50 keV). The blackening of the film inside the reactor would, in that case, be due to bremsstrahlung caused by the deceleration of electrons in the lead foil generating photons of energy limited to some 50 keV; these photons would thus be capable of passing through 125 μm of lead, but not through 4 mm of Pyrex, leaving the film outside the reactor intact. Note that such film blackening has also been observed after loading hydrogen or deuterium in palladium by a plasma focus device[24] and has been attributed to low-energy electrons.

VII.A.4. Conclusions of the October–November 1989 Radiation Measurement

The most obvious conclusion of this assessment is that there is no evidence of the three monitored nuclear reactions: No gamma photons were detected, and the production of neutrons and tritium (if any) is many (ten) orders of magnitude lower than would be expected. The only sign of nuclear activity seems to be low-energy beta activity, the electrons having, in the case of the experiments with deuterium, a maximum energy of ~50 keV. More arguments in favor of this hypothesis are given later.

VII.B. June–July 1992 Assessment

To obtain more precise information on the cause of the X-ray film blackening, we modified our reactor slightly to enable easy detection of any ionizing radiation emitted by the palladium after its activation by sparking.

VII.B.1. Detection Devices Installed

The reactor was modified in the following way:

1. The copper points are now supported by a 1-mm-thick × 6-cm-diam × 10-cm-high lead cylinder instead of by a copper disk.

2. The copper tube supporting the palladium can be directly connected to ground through connection D2.

An auxiliary dc generator (with output voltage tunable between 0 and 300 V) is installed close to the reactor, according to Fig. 23a.

The protocol used is the following:

1. The palladium, after having been subjected, in a separate vessel, to hydrogen or deuterium pressure cycles (between 10 mb and 20 bars) at 200°C, is activated by sparking under conditions used in previous experiments, for 24 to 48 h (it had been checked in a preliminary experiment that film blackening occurred). The experimental setup is shown in Fig. 23a.

2. After this activation, the high-voltage generator is cut off and disconnected (time $t = 0$), and the other connections installed as shown in Fig. 23b (before we connect A1 to A2, A1 is connected to ground to eliminate any electrical charge present on the lead cylinder). We now have a proportional counter, capable of detecting any ionizing radiation present in the gaseous gap between the electrodes, by measuring the current flowing in the circuit (by measuring the voltage drop across the 500-kΩ resistance after opening bypass BP2).

VII.B.2. Results of the Radiation Measurements

Before we ran experiments with hydrogen isotopes, reference experiments were run:

1. A virgin palladium cathode, under a polarization voltage of 300 V, yielded a voltage difference of <0.1 mV across the 500-kΩ resistance (current <0.2 nA).

2. A palladium cathode, after being subjected to sparking in argon for 4 days, yielded, under a polarization voltage of 300 V, a voltage difference of <0.1 mV.

3. A palladium cathode, after being subjected to sparking in nitrogen for 2 days, yielded, under a polarization voltage of 300 V, a voltage difference of <0.1 mV.

4. After activation by sparking in hydrogen or deuterium, a palladium cathode was completely regenerated by being heated in air at 1100°C for 15 min. Subjected to procedure 2, it yields the same background value for the voltage difference (0.1 mV).

VII.B.2.a. Case of deuterium: Figure 24a gives the evolution of the voltage drop for a palladium cathode activated by sparking for 48 h in deuterium (900 mb). The conditions during the voltage drop measurement were as follows:

1. reactor pressure: 865 ± 3 mb.

2. polarization voltage: 99 ± 0.2 V, positive polarity.

3. cabin temperature: 22 ± 0.5°C.

It can be seen from Fig. 24a that after a short period of some 10 min, when the voltage drop increases from 100 to nearly 400 mV, its general tendency is an exponential decrease with time, to reach 35 mV after 400 min; during this decrease, bursts of current are observed that are particularly high in amplitude (in this case) between 50 and 100 min. Figure 24b

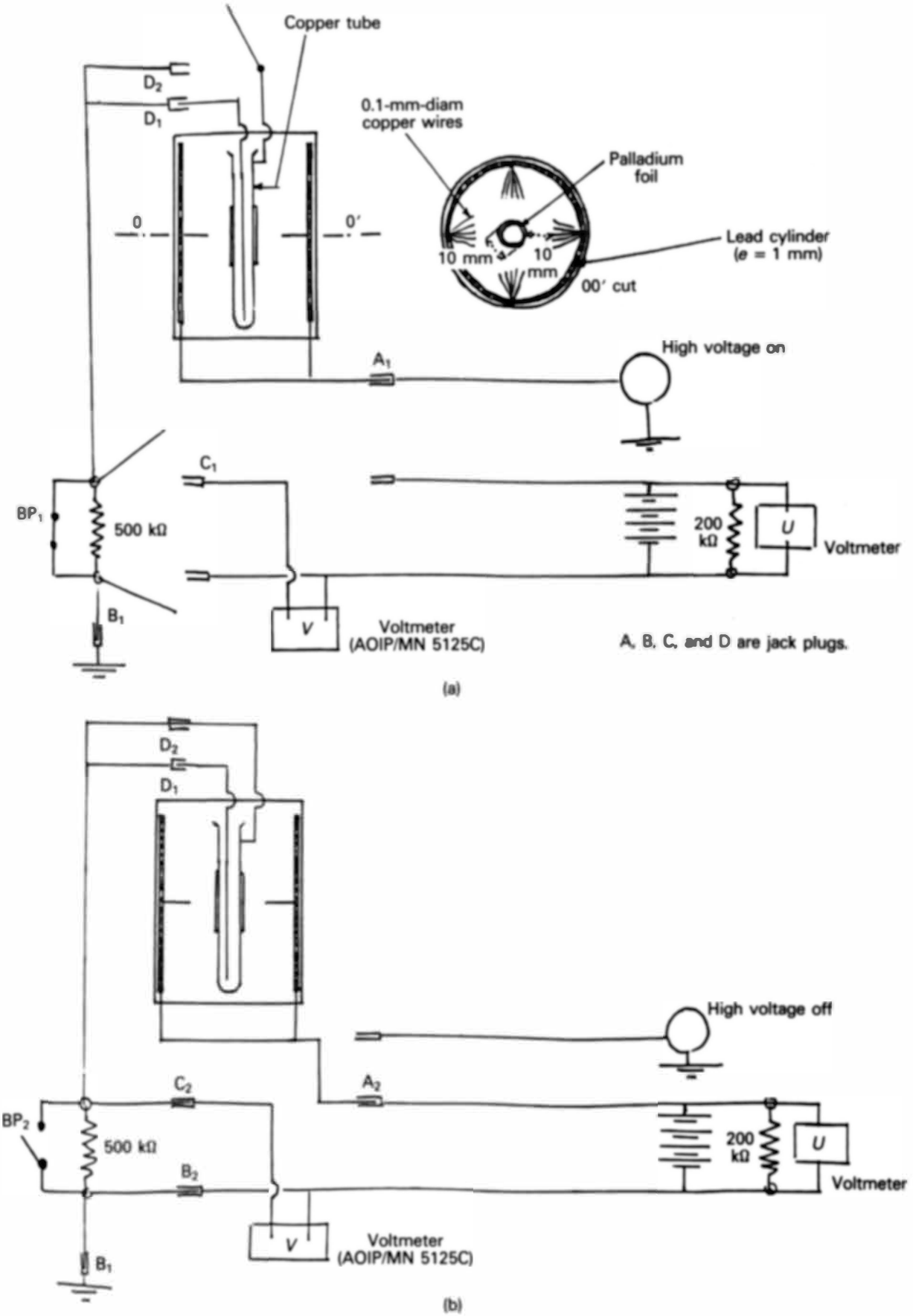

Fig. 23. (a) Palladium activation and (b) radiation measurement.

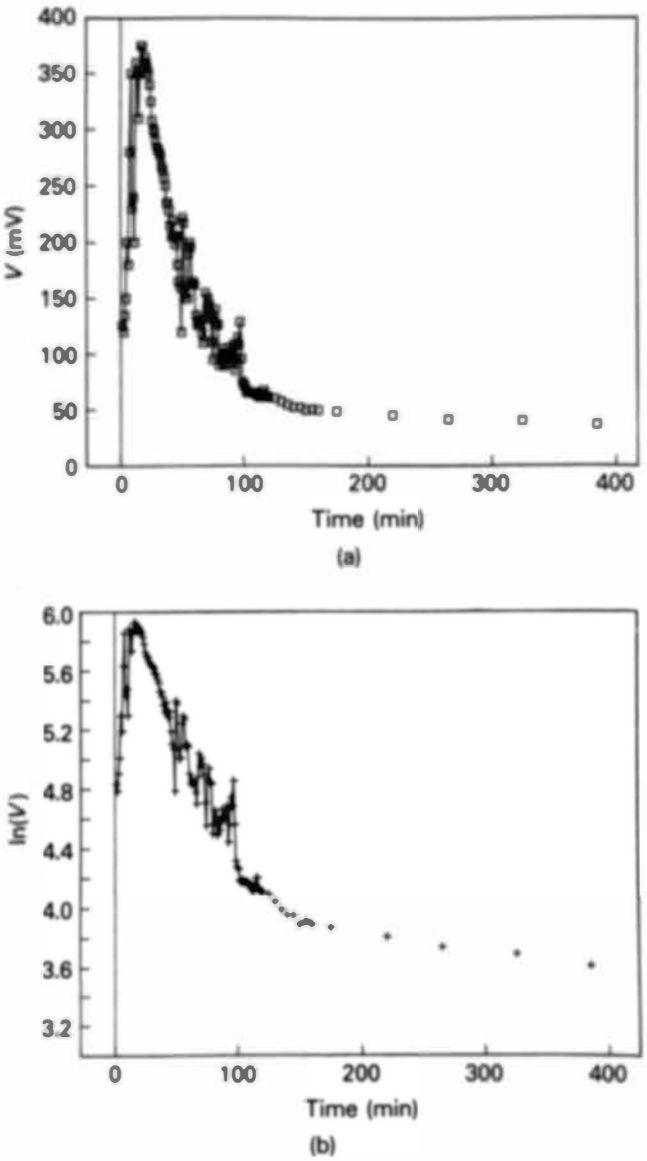

Fig. 24. (a) Radiation emission from a deuterium-palladium system and (b) half-life of radiation emitted.

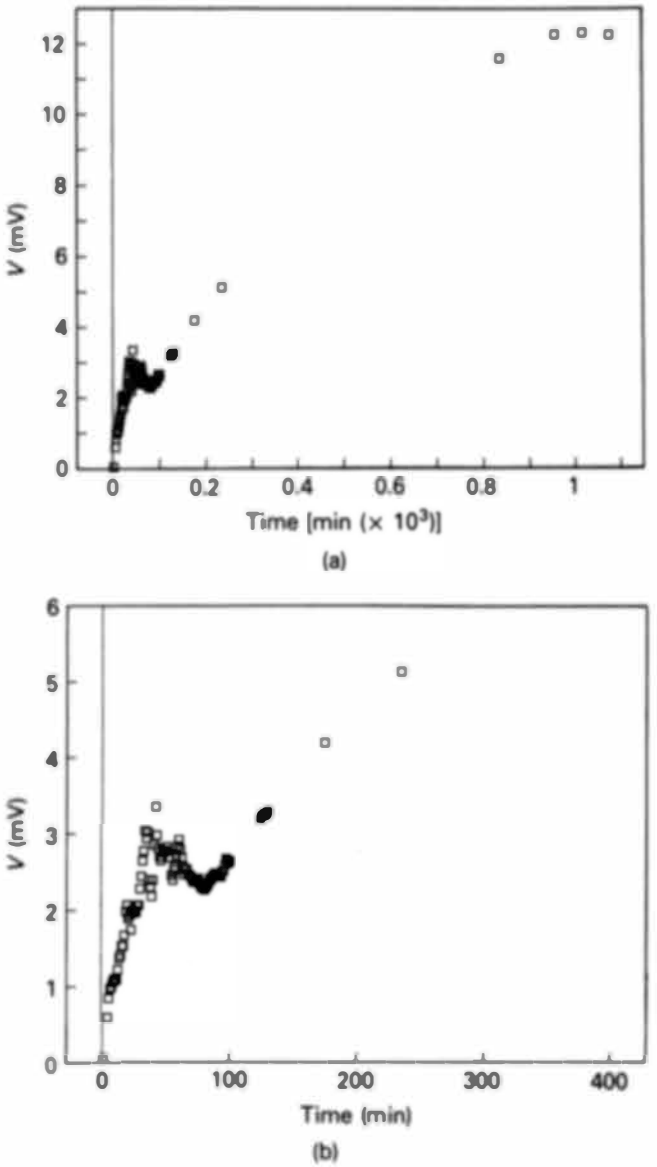

Fig. 25. (a) Radiation emission from a hydrogen-palladium system and (b) enlarged view.

gives ln(V) as a function of time. It can be seen that two straight lines can be drawn in this graph: one between 0 and 100 min, corresponding to a half-life of 20 min, and a second one between 150 and 400 min, corresponding to a half-life of 10 h.

Three measurements were done with peak voltage ranging from 100 to 750 mV and half-life ranging from 17 to 24 min (first decrease) and between 6 to 12 h (second decrease).

VII.B.2.b. Case of hydrogen: Figure 25a gives the evolution of the voltage drop for a palladium cathode activated by sparking for 24 h in hydrogen (900 mb). The conditions during the voltage drop measurement were as follows:

1. reactor pressure: 830 ± 8 mb
2. polarization voltage: 99 ± 0.2 V, positive polarity
3. cabin temperature: 22 ± 0.5°C.

It can be seen from Figs. 25a and 25b (enlargement) that the behavior is different from the deuterium case. The voltage is much lower (maximum 12 mV), and the evolution is completely different: After a period of some 40 min of rapid rise, the voltage drops for some 60 min and then rises again with a lower slope to reach a steady-state plateau after some 12 h. The half-life of the decrease observed between 40 and 100 min has been estimated to be ~20 min.

The plateau is still observed after 5 days. At that time, pumping out the reactor gas phase and replacing it by fresh hydrogen (three times) causes the voltage to drop to zero.

Two measurements were done, with plateau values of 6 and 12 mV, respectively. The short half-life decrease was observed only in the 12-mV experiment. The same behavior was observed when the reactor was plumped out.

This ionization of the gas gap between the electrodes cannot be due to hydrogen isotopes leaving the palladium electrode as ions: It is well established that hydrogen desorbs

from a metal as molecular hydrogen. It is most likely due to electrically neutral species having a nuclear ionizing activity (beta emission; see Sec. VIII.D).

VII.B.3. Conclusions of the June–July 1992 Radiation Measurements

The information disclosed by these measurements is discussed in Sec. VIII.D.

VIII. DISCUSSION

A number of phenomena have to be taken into account to form a hypothesis capable of explaining (at least qualitatively) the experimental results obtained. Among these, some are physical or chemical in nature and are related to the complex hydrogen isotope-metal system built by the action of the sparks. Others might be nuclear in nature, involving fusion reactions, implying hydrogen isotopes in the metal. These reactions are not likely to be classical because the absence of the usual by-products.

To clarify the discussion, we first describe briefly the main features of the sparks used and then indicate the type of dynamic hydrogen isotope-metal system they can build. We then propose a nonclassical class of nuclear reactions that can explain the experimental observations.

VIII.A. Characteristics of tha Sparks

The sparks used in our study are high-frequency sparks, as can be seen in Fig. 8, where the time at which they occur is indicated. They are typically impulse-voltage sparks (rate of voltage rise before sparking is 1000 V/μs); that is, there is no appreciable accumulation of space charges in the gap. Before the onset of the sparks, negative feathers (in the case of negative points) or positive streamers (in the case of positive points) fill the gap and create high transient electrical fields close to the surface of the metal. When breakdown occurs, the spark canal is filled with atomic hydrogen, and an intense current flows from the metal to the gas. Typically, sparking lasts some 50 μs in each cycle (when an average of five sparks occur), and there are F cycles per second, where F is the frequency used to trigger the ignitor. In all experiments, F was equal to 310 Hz.

VIII.B. Possible Dynamic Hydrogen-Metal System

We now examine the dynamic system that may be developed by the action of sparks on the metal of the electrodes when hydrogen is present in the reactor (hydrogen meaning any hydrogen isotope). Figure 26 gives a schematic representation of the succession of these events (in the case of Fig. 26, sparks occur when the points are negative):

1. During sparking, atomic hydrogen generated in the spark canal diffuses toward the surface of the electrode and penetrates the metal to form a hydride or a supersaturated solution. Measurements of reactor pressure variations at the start of the experiment give a D/Pd ratio of 0.70 when palladium is used as the electrode. It is generally accepted that at least part of the hydrogen present in conductive hydrides is in the form of protons; their electrons are shared in the conduction band of the metal, and the remainder are either hydrogen atoms or negative hydrogen ions.

2. At each spark occurrence, a pulse of current of high intensity flows in the spark canal and in the metal of the electrode. The mean value J of the intensity of this pulse can be estimated from the measurement of the average intensity i of the current flowing in the coil secondary (5 mA), the duration of one spark (1 μs,) and the number of sparks per second (five sparks per cycle and 310 cycle/s). The order of magnitude of J is thus 2 A. This pulse current flows through a very small section S of the metal of the electrode (typically 10^{-7} cm^2). If we assume that this section is the same through the hydride layer of the metal, the amplitude $|E|$ of the transient electrical field created in the metal by the spark can be estimated to be

$$|E| = rj \ , \tag{9}$$

where

$j = J/S$

r = resistivity of the metal.

For palladium, $|E|$ = 120 V/cm, which is considerably higher than the values observed for the usual currents flowing through metals, which are of the order of 0.01 V/cm. (Note that similar high transient fields in the metal are likely to be produced by feathers—or streamers—occurring before the onset of the sparks.)

This transient field accelerates the conduction electrons of the metal and the protons that are in it. During this motion, protons experience many collisions (some of them of nuclear size) with electrons in the metal (either conduction or bound ones). The collision rate is considerably increased by the high transient electrical field in the metal. This is a major difference with the situation existing, for example, in electrolysis experiments and in experiments using a glow discharge at low pressure, with palladium electrodes.[14]

To summarize, we can visualize the possible dynamic hydrogen-metal system as a fluctuating layer of protons in the metal, formed from the atomic hydrogen generated by the sparks and pulsewise accelerated in this metal by transient electrical fields caused by the sparks (note that a comparable situation exists when the points are positive).

VIII.C. Proposed Class of Nuclear Reactions

An explanation has recently been put forward[25] that relates the excess energy produced to tightly bound chemical states of hydrogen isotopes (D_2 and H_2) in metals. This effect might contribute to the excess energy we observe.

Nevertheless, because heat release is observed in our system for both hydrogen and deuterium, together with radiation emission that remains long after sparks are cut off, we propose a possible class of cold fusion reactions that works with all hydrogen isotopes and explains the radiation emission. We think these reactions are likely to make an important contribution in our setup.

For hydrogen, two reactions are known in the sun and are the first steps of the proton cycle:

$$p + p = d + e^+ + \text{neutrino} \quad (+1.442 \text{ MeV}) \tag{10}$$

and

$$p + p + e^- = d + \text{neutrino} \quad (+1.442 \text{ MeV}) \ . \tag{11}$$

We note that both reactions imply only the weak electronuclear force to dispose of the excess energy. The second one yields only a deuteron and a neutrino, meaning that nearly all the energy is carried away by the neutrino; the deuteron carries only the recoil energy (0.001 MeV).

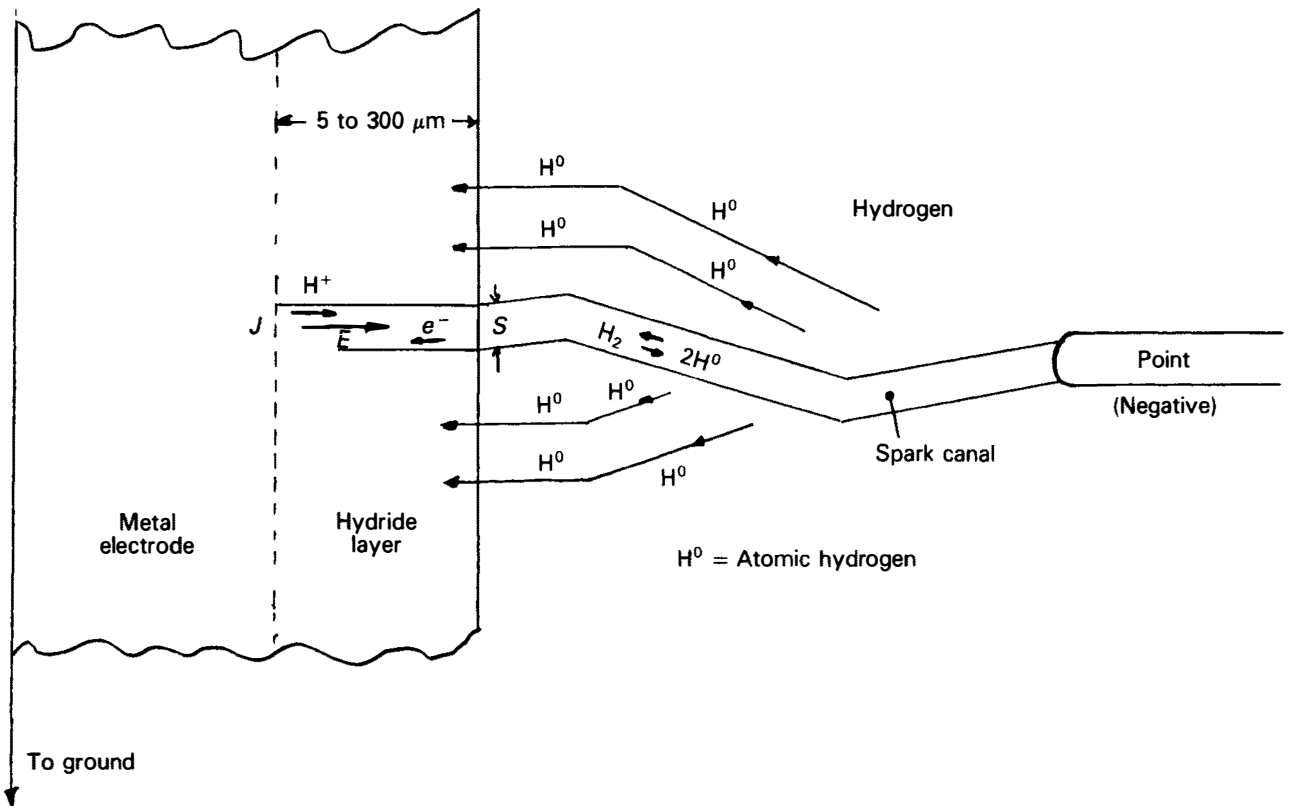

Fig. 26. Conceptual model.

We now refer to the fluctuating layer of protons colliding with electrons in the metal of the electrode as previously described, and we consider the system formed by two protons and one electron on their way to a three-body collision (this type of collision is likely to happen, owing to the very high concentration of electrons and hydrogen in the metal, the periodic nature of the metal in the solid state, and the high value of the transient electrical field that increases the rate of collisions). This is one state of this ($p + p + e$) system, which we call state 1. The system has two other possible states.

State 2 (d + neutrino) has the same energy level as state 1 because the reaction ($p + p + e^- = d$ + neutrino) is exothermal (+1.442 MeV). We nevertheless note that this reaction is impossible at room temperature because of the Coulomb barrier to be overcome.

State 3 ($p + n$ + neutrino) has a higher energy level than state 1 because the reaction ($p + e^- = n$ + neutrino) is endothermal by 0.782 MeV.

Figure 27 is a schematic representation of the three states of this physical system. Because of the principle of energy conservation, this system could have a direct transition from state 1 ($p + p + e$) to state 2 (d + neutrino), provided its various elements can interact. But, owing to the Coulomb barrier, this is not the case, and a direct transition from reaction (10) to (11) is impossible.

However, because of a very general mechanism, revealed by quantum mechanics, this transition can occur indirectly (with a certain probability) by the intermediate passage through state 3 ($p + n$ + neutrino). This state violates the principle of energy conservation and is not observable. It is

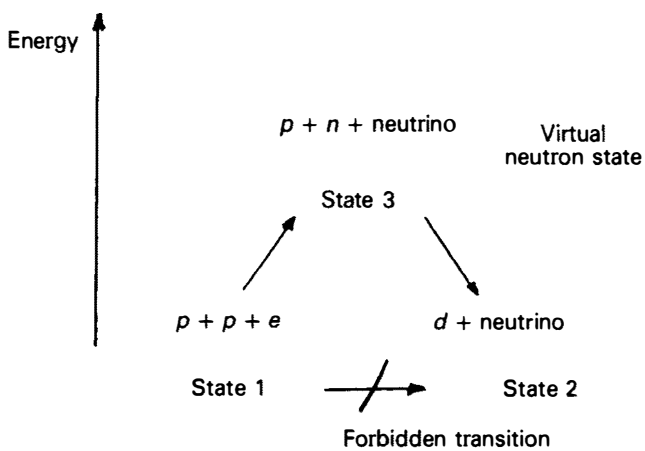

Fig. 27. Proton-proton-electron system.

a virtual state of the system. (Note that in contrast to Ref. 18, no hypothesis is made on the rest mass of the neutrino.)

This is a reaction completely different from the direct one observed at much higher energies of the protons [reaction (10)], in which the Coulomb barrier is overcome by kinetic energy. To make this last point even more clear, we now examine the next reaction likely to occur in our system (when hydrogen is processed), by comparison with what happens in the sun:

$$p + d = {}^3\mathrm{He} + \gamma \ . \qquad (12)$$

In this case, it is the proton that reacts with the deuteron. The fusion energy released is carried away by a gamma photon.

In our system,

$$p + e^- + d = t + \text{neutrino} \ . \qquad (13)$$

In this case, it is the virtual neutron that reacts with the deuteron (or the virtual dineutron with the proton). The fusion energy released is carried away by the neutrino. The tritium formed (which is too rich in neutrons) subsequently re-equilibrates by β^- emission, finally yielding ^{3}He.

When deuterium is processed, the reaction corresponding to reaction (11) would be

$$d + d + e^- = {}^4\text{H} + \text{neutrino} \ . \qquad (14)$$

Hydrogen-4 is an unstable isotope of hydrogen. We think its formation is possible under our conditions because the neutrino required to carry away the large excess of energy of reaction (14) (some 23 MeV) is present in the reacting nucleus, meaning that de-excitation can occur through neutrino emission, in typical nuclear time (1×10^{-22} s). This unstable hydrogen isotope would quickly deactivate by β^- emission, according to

$$^4\text{H} = {}^4\text{He} + e^- + \text{neutrino} \ . \qquad (15)$$

The detailed mechanisms involved in the sequence of reactions (14) and (15) will, in any case, have to be elucidated.

Before analyzing the evidence that supports the general hypothesis we propose (results of the June–July 1992 radiation measurement series), we make a general comment: The four examples quoted illustrate the four main features of the class of nuclear reactions we propose as a possible explanation of cold fusion when triggered by sparking in hydrogen isotopes:

1. The Coulomb barrier is avoided by an indirect transition of second-order approximation.

2. The daughter nucleus is neutron rich and, if unstable, will preferentially stabilize through β^- emission.

3. The final products of the reactions are likely to be complex mixtures resulting from the various possible (and successive) reactions between hydrogen isotopes and their corresponding virtual neutron states. Because of the successive reactions occurring, the composition of these mixtures is likely to be very dependent on the time of sampling in the course of an experiment. Besides, other nuclei present in the metal can react with virtual neutron states.

4. Most of the fusion energy released is carried away by neutrinos and is thus definitively lost. Only the recoil energy of the daughter nucleus is left in the reactor.

This last point sounds a bit pessimistic. In fact, it is not, for the following two reasons:

1. In the case of the $(p + p + e^-)$ reaction, the recoil energy is already some 400 times the combustion energy of the hydrogen atom. This recoil energy is proportional to the square of the energy carried away by the neutrino and inversely proportional to the mass of the daughter nucleus. In the case of the $(d + d + e^-)$ reaction, the recoil energy can thus be evaluated to be 60 000 times the combustion energy of hydrogen [this figure is 6000 for the $(p + d + e^-)$ reaction].

2. Combining the facts that the $(p + p + e^-)$ reaction yields deuterium and that the $(d + d + e^-)$ reaction has a much higher recoverable energy release shows the potential of these successive reactions to yield energy, starting from common hydrogen, with only low-energy beta rays as by-products.

VIII.D. Evidence in Favor of This Hypothesis to Explain Cold Fusion Reactions Triggered by Sparking

We now refer to the results of the June–July 1992 radiation assessment reported in Sec. VII.B. The current observed in the counter can be due to any ionizing radiation present in the gap (photons, electrons, protons, alpha particles, etc.). However, observations made tend to favor the hypothesis of electrons (β^- radiation), emitted by gaseous species, capable of diffusing out of the palladium lattice (as shown by the regeneration procedure used). We now discuss these observations and show that they fit qualitatively our hypothesis on fusion reactions involved in sparking experiments.

VIII.D.1. Deuterium

In the case of deuterium, the cold fusion reactions we propose are the following:

$$d + d + e^- = {}^4\text{H} + \text{neutrino} \quad (Q \sim 23 \text{ MeV}) \qquad (16)$$

followed by

$$^4\text{H} = {}^4\text{He} + e^- + \text{neutrino} \quad (Q \sim 50 \text{ keV}) \ . \qquad (17)$$

The way in which the film blackening occurred in our experiments is compatible with β^- from reaction (16) having an energy around 50 keV.

The half-life of the unstable ^{4}H from reaction (17) would be 20 min, as indicated by Fig. 24b.

To explain the shape of the voltage curve as a function of time (see Fig. 24a), we first note that a few micrometres of metal would drastically decrease the energy of β^- electrons emitted by reaction (17) before they reach the gaseous gap between the electrodes, thus reducing the number of ionizations they can produce in the gas and the current flowing in the circuit.

We now turn to the system formed by the palladium subjected to sparking in deuterium: The high atomic deuterium pressure existing at the surface of the palladium tends to maintain, inside the palladium, ^{4}H formed by reaction (16) (note that this could yield an underestimation of the energy of the emitted betas when film blackening during sparking is used as a way of measuring it).

When sparking ceases, ^{4}H can diffuse at a higher rate toward the surface, thus increasing the voltage until a steady state is reached, when the evolution of voltage is ruled by the half-life of ^{4}H. Bursts observed in the evolution of voltage can be due to heterogeneity in the palladium, resulting in an irregular diffusion of ^{4}H toward the surface. The second part of the evolution of voltage is less clear and may be due to a different regime of ^{4}H diffusion out of the palladium lattice.

It is, for the time being, very difficult to give a quantitative interpretation of the results (on the one hand, the amplification of the proportional counter is not known, and, on the other, neither is the rate of recovery of the emitted β^-). Nevertheless, an order of magnitude of the β^- electrons produced can be obtained, by extrapolating the voltage to $t = 0$. This gives a value of 660 mV, corresponding to a current of 1.35 μA.

The number of electrons collected in the counter is thus 1.0×10^{13}/s. This figure is what would be expected for an

excess energy of 2 W generated by reaction (10) when only the recoil energy (0.29 MeV) is left in the reactor.

VII.D.2. Hydrogen

In the case of hydrogen, the cold fusion reactions we propose are the following:

$$p + p + e^- = d + \text{neutrino} \quad (18)$$

followed by

$$p + d + e^- = t + \text{neutrino} \quad (19)$$

when the concentration of deuterons from reaction (18) has sufficiently increased. If the concentration of tritons increases sufficiently, the next reaction can occur:

$$p + t + e^- = {}^4\text{H} + \text{neutrino} \; . \quad (20)$$

We note that because tritium has a half-life of 12.3 yr, the emission of β^- would be much smaller than from a beta emitter with a 20-min half-life (for a comparable number of nuclei present in the reactor). Moreover, a decline in activity would not be detected in a few hours. We thus attribute the 12-mV plateau, reached after some 12 h, to tritium that has diffused out of the palladium, according to an exponential law with time (see Fig. 25a).

We now turn to the small peak observed during the first 100 min, which starts with a higher slope than the general trend (see Fig. 25b, which is an enlargement of this period). We attribute this peak to small amounts of ^{4}H formed: Its activity decreases with a half-life comparable with that observed with deuterium as a starting gas (20 min).

The fact that the activity falls to zero when the gas is pumped out confirms that this activity is due to species that can diffuse through the palladium (hydrogen isotopes).

Note that the experimental search for tritium was made in a deuterium experiment where the formation of tritium is not expected.

IX. CONCLUSIONS

Sparking in hydrogen isotopes (H_2 and D_2) between electrodes of various metals (palladium, stainless steel) yields, in the setup we have used, an excess energy production that is fully reproducible and stable over very long periods. No systematic errors have been found that could explain the statistically significant excess energy production we have measured in comparison with reference experiments.

A possible explanation of the facts we have observed is a hypothetical class of cold fusion reactions between hydrogen isotopes. The application of the principles of quantum mechanics to the three-body collision of two hydrogen isotopes and one electron shows that this system can end up in the state of one neutron-rich hydrogen isotope and a neutrino, with an observable probability, through an indirect transition (virtual neutron + neutrino state of the system). The direct transition is, of course, forbidden by the Coulomb barrier. These reactions occur at room temperature and imply the action of the weak electronuclear force.

The rate at which these reactions can occur is, of course, strongly dependent on the probability of three-body collisions of nuclear size. This probability is extremely low in the sun's plasma despite its very high density (mean distance between particles is 0.3 Å). This can be explained (in an elementary way) by the very high thermal energy of the particles, which prevents the Coulomb forces from deviating their trajectories, in this way increasing the collision cross section. Moreover, most of these improbable collisions are inefficient because the contact time is too low for the weak nuclear force to act. Low-temperature plasmas (3000 K) are also very inefficient for favoring three-body collisions: In that case, the thermal energy is low, but the distance between particles is so high (70 Å) that deionization is the dominant process. In contrast, the periodic nature of the host metal, the high concentration of low-thermal-energy protons and electrons in it, at a mean distance of ~2 Å, and the motions of these particles induced by the transient electrical field are likely to increase considerably the probability of three-body collisions, in the case of cold fusion in metals. Moreover, the contact time of these collisions can be estimated (in an elementary way) to be $\sim 10^{-12}$ to 10^{-14} s, which is the order of magnitude of the characteristic time of the weak nuclear force.

It is our objective to gather more experimental evidence to support our hypothesis on cold fusion reactions occurring under our experimental conditions, to measure the rate at which these reactions occur, and to identify precisely their by-products (radiations, ^{4}He, etc.).

This effort will show whether cold fusion triggered by sparking in hydrogen isotopes has a future in the field of energy production.

REFERENCES

1. S. E. JONES et al., "Observation of Cold Nuclear Fusion in Condensed Matter," *Nature*, **338**, 739 (1989).

2. M. FLEISCHMANN and S. PONS, "Electrochemically Induced Nuclear Fusion of Deuterium," *J. Electroanal. Chem.*, **261**, 301 (1989).

3. J. TANDBERG, "A Method for Producing Helium," Swedish Patent Application (1927).

4. F. PANETH and K. PETERS, "Uber die Verwandlung von Waterstoff in Helium," *Naturwissenschaften*, **14**, 958 (1926).

5. R. DAGANI, "Hopes for Cold Fusion Diminish as Ranks of Disbelievers Swell," *Chem. Eng. News*, **8** (May 22, 1989).

6. Y. ARATA and Y. C. ZHANG, "Achievement of an Intense Cold Fusion Reaction," *Fusion Technol.*, **18**, 95 (1989).

7. P. K. IYENGAR et al., "Bhabha Atomic Research Center Studies in Cold Fusion," *Fusion Technol.*, **18**, 32 (1989).

8. L. ZAHM et al., "Experimental Investigations of the Electrolysis of D_2O Using Palladium Cathodes and Platinum Anodes," *J. Electroanal. Chem.*, **281**, 313 (1990).

9. P. PERFETTI et al. "Neutron Emission Under Particular Non-Equilibrium Conditions from Pd and Ti Electrolytically Charged with Deuterium," *Nuovo Cimento D*, **11**, *6*, 921 (1989).

10. A. DE NINNO et al., "Evidence of Emission of Neutrons from a Titanium-Deuterium System," *Europhys. Lett.*, **9**, *8*, 221 (1989).

11. S. AIELLO et al., "Nuclear Fusion Experiment in Palladium Charged by Deuterium Gas," *Fusion Technol.*, **18**, 115 (1990).

12. A. GU et al., "Preliminary Experimental Study on Cold Fusion Using Deuterium Gas and Deuterium Plasma in the Presence of Palladium," *Fusion Technol.*, **16**, 248 (1990).

13. D. RUZIC et al., "A Novel Apparatus to Investigate the Possibility of Plasma Assisted Cold Fusion," *Fusion Technol.*, **16**, 253 (1989).

14. Y. R. KUCHEROV et al., "Nuclear Product Ratio for Glow Discharge in Deuterium," *Phys. Lett. A*, **170**, 265 (1992).

15. B. CROWLEY, "Nuclear Fusion in High Density Matter," *Nucl. Fusion*, **29**, 2199 (1989).

16. A. LEGGETT and G. BAYM, "Can Solid State Effects Enhance the Cold Fusion Rate," *Nature*, **340**, 45 (1989).

17. J. RAFELSKI et al., "How Cold Fusion Can Be Catalyzed," *Fusion Technol.*, **18**, 136 (1989).

18. J. RUSSELL, "Virtual Electron Capture in Deuterium," *Ann. Nucl. Energy*, **18**, *2*, 75 (1991).

19. J. BOUDARD, "The Virtual Pressure of Atomic Hydrogen in a Palladium Cathode Away from Equilibrium," *Comm. Catalyt. Highlights* (Mar. 29, 1989).

20. R. BALIAN et al., "Cold Fusion in a Dense Electron Gas," *J. Phys. France*, **50**, 2307 (1989).

21. E. STORMS, "Review of Experimental Observations About the Cold Fusion Effect," *Fusion Technol.*, **20**, 433 (1991).

22. J. DUFOUR, "Energy Source System," Patent Application WO91/01036 (1991).

23. M. SRINIVASAN et al., "Tritium and Excess Heat Generation During Electrolysis of Aqueous Solutions of Alkali Salts with Nickel Cathode," Preprint, Conf. Cold Fusion, Nagoya, Japan, October 21-25, 1992.

24. R. K. ROUT, A. SHYAM, M. SRINIVASAN, and A. BANSAL, "Copious Low Energy Emissions from Palladium Loaded with Hydrogen or Deuterium," *Indian J. Technol.*, **29**, 571 (1991).

25. J. P. VIGIER, "New Hydrogen Energies in Specially Structured Dense Media," Preprint, Conf. Cold Fusion, Nagoya, Japan, October 21-25, 1992.